Production of super-heavy nuclei in cold fusion reactions

V. Yu. Denisov[1,2†] I. Yu. Sedykh[3]

[1]Institute for Nuclear Research, Prospect Nauki 47, 03028 Kiev, Ukraine
[2]Faculty of Physics, Taras Shevchenko National University of Kiev, Prospect Glushkova 2, 03022 Kiev, Ukraine
[3]Financial University under the Government of the Russian Federation, Leningradsky Prospekt 49, 125993 Moscow, Russian Federation

Abstract: A model for cold-fusion reactions related to the synthesis of super-heavy nuclei in collisions of heavy projectile-nuclei with a ^{208}Pb target nucleus is discussed. In the framework of this model, the production of the compound nucleus by two paths, the di-nuclear system path and the fusion path, are taken into account simultaneously. The formation of the compound nucleus in the framework of the di-nuclear system is related to the transfer of nucleons from the light nucleus to the heavy one. The fusion path is linked to the sequential evolution of the nuclear shape from the system of contacting nuclei to the compound nucleus. It is shown that the compound nucleus is mainly formed by the fusion path in cold-fusion reactions. The landscape of the potential energy related to the fusion path is discussed in detail. This landscape for very heavy nucleus-nucleus systems has an intermediate state, which is linked to the formation of both the compound nucleus and the quasi-fission fragments. The decay of the intermediate state is taken into account in the calculation of the compound nucleus production cross sections and the quasi-fission cross sections. The values of the cold-fusion cross sections obtained in the model agree well with the experimental data.

Keywords: super-heavy nuclei production, statistical compound-nucleus reactions, low energy heavy-ion reactions, fusion and fusion-fission reactions

DOI: 10.1088/1674-1137/abdfc0

I. INTRODUCTION

The synthesis of super-heavy nuclei (SHN) is a very interesting, exciting and puzzling physical task, as much for experimentalists as for theoreticians. The elements beyond Md, with proton numbers $Z = 102 - 118$, have been synthesized by the fusion of heavy nuclei [1-27]. The element Og, with $Z = 118$, is the heaviest element which has been synthesized to date, discovered by Oganessian *et al*. [1, 24]. Recently, experiments aimed at the synthesis of isotopes of elements $Z = 119$ and 120, or at the study of properties of related reactions, have been performed [28-34], but no decay chains consistent with the fusion-evaporation reaction products have been observed.

Cold-fusion reactions for SHN synthesis are reactions between heavy-ion projectiles with mass/charge $A \geqslant 48/Z \geqslant 20$ and lead or bismuth targets. This type of reaction was proposed by Oganessian *et al*. [35]. Using these reactions, SHN with charges Z = 102÷113 have been successfully synthesized in experiments [2-22].

Many different models have been proposed to describe the cross section of the synthesis of SHN in heavy-ion collisions; see, for example, Refs. [27, 36-89] and papers cited therein. The common feature of the models is that the cross section of SHN production is described as the product of the capture cross section, the probability of compound nucleus formation, and the survival probability of the compound nucleus. The capture process is related to the formation of the system of touching nuclei. The probability of compound nucleus formation is connected to the process of the evolution from the system of contacting nuclei to the spherical or near spherical compound nucleus. The survival probability of the compound nucleus is linked to the competition between the fission and neutron emission processes. When the excitation energy of a compound nucleus drops, the residue nucleus emits alpha-particles and/or divides into two fission fragments, which can be detected in experiments. The chain of alpha-particles and/or the fission fragments observed in the experiment are the experimental signals of successful synthesis of SHN [1-27].

The differences between various models [36-89] in the description of the capture process are related to the different nucleus-nucleus interaction potentials used, consideration of different shapes and mutual orientations of interacting nuclei, and applications of various approximations in the evaluation of the capture cross sections. The differences of various models in the description of the survival probability are connected to the different statist-

Received 22 October 2020; Accepted 29 December 2020; Published online 20 February 2021
† E-mail: denisov@kinr.kiev.ua

ical nuclear decay models applied, various expressions for the energy level densities, different values for the fission barrier of the SHN obtained in the frameworks of various nuclear structure models, various dependencies of the fission barrier on the excitation energy of the compound nucleus, and different values of the neutron binding energy taken from various nuclear mass models. Consequently, the corresponding differences between the results obtained in the frameworks of various approaches to the capture cross-section and the survival probability of the compound nucleus are natural, reasonable and understandable. The physical mechanisms of the capture cross-section and the survival probability of the compound nucleus are the same in the different models.

The process of compound nucleus formation from the two touching nuclei during the synthesis of SHN is the most undefined up to now, because there are two alternative mechanisms for this process, the fusion [36-58] and di-nuclear system (DNS) [59-76, 76, 78] mechanisms, which are under active discussion.

The fusion approach to compound nucleus formation is related to the smooth subsequent shape evolution from the system of two touching nuclei to the compound nucleus, see Refs. [36-58] and papers cited therein. The models considered in Refs. [36-58] are based on different approaches to the shape evolution and/or the shape parametrization of the nuclear system during the compound nucleus formation. The compound nucleus formation is in competition with the quasi-fission and deep-inelastic processes in the framework of the fusion approach.

The alternative mechanism of compound nucleus formation from the two colliding nuclei was proposed by Volkov in Ref. [59]. This mechanism is related to the evolution of a DNS formed by the two contacting nuclei after penetration through the fusion barrier of the incident nuclei. In the framework of the DNS model, the compound nucleus is formed by multi-nucleon transfer from the light nucleus to the heavy one. The transfer of nucleons in the opposite direction (from the heavy nucleus to the light one) as well as the decay of the DNS through the fusion barrier, are the processes competing with the compound nucleus formation. Both nuclei touch each other during these multi-nucleon transfers. This DNS mechanism of the compound nucleus formation is applied to SHN production in Refs. [59-78]; see also papers cited therein.

Note that the same experimental values of the production cross section of SHN can be described by applying various approaches for the compound nucleus formation. However, the fusion and DNS mechanisms of compound nucleus formation are very different. It should also be noted that the probability of compound nucleus formation can also be evaluated by various phenomenological or semi-phenomenological expressions [36-38, 44, 46, 79-88].

The DNS approach was first successfully applied to a description of deep inelastic heavy-ion collisions [90]. In this case, two nuclei collide at high energies and form a fast-rotating DNS. The fast rotation of the DNS prevents the fusion of the two nuclei and stabilizes the rotating DNS, because the potential of the rotating DNS is repulsive at small distances between nuclei, due to the contribution of the centrifugal force. Therefore, multi-nucleon exchange between the fast-rotating nuclei forming the DNS naturally takes place during deep inelastic heavy-ion collisions. After rotation by some angle, the DNS decays into two excited nuclei, which have other nucleon compositions and smaller values of the relative kinetic energies than the incident nuclei [90].

Cold fusion reactions take place at collision energies near the barrier of the nucleus-nucleus potential [91, 92]. Therefore, the possible frequency of rotation of the DNS formed in SHN formation reactions is much smaller than in deep inelastic heavy-ion collisions. Therefore, stabilization of the DNS due to rotation is impossible for heavy-ion systems leading to SHN. Another possibility for the formation of the barrier at small distances between ions is a diabatic behaviour of nuclear levels during fast collisions [93]. The diabatic shift of heavy-ion potential energy occurs when the relative velocity of heavy ions is very high, so nucleons occupy diabatic levels and cannot quickly relax in time to the adiabatic ones. However, the relative velocity of ions disappears during the penetration of the fusion barrier, and the evolution of the dinuclear system is related to small relative velocities. The potential energy surfaces obtained in the framework of various microscopic or semimicroscopic calculations have not shown the barrier for reactions related to SHN synthesis [40, 43, 45, 47, 48, 51-56]. Nevertheless, the DNS potential calculated in Refs. [60-78] shows strong repulsion at small distances between nuclei, which stabilizes the DNS system in this model. Such behaviour of the DNS potential in Refs. [60-78] is related to the calculation of the nucleus-nucleus potential in the frozen-density approach. The frozen-density nucleus-nucleus potential is strongly repulsive at small distances between nuclei, because the frozen nucleon densities of the colliding nuclei overlap well at such distances and form a high-density region [91, 92]. Due to the high value of the incompressibility of nuclear matter, the potential energy of nucleus-nucleus systems rises dramatically when the nucleon density becomes higher than the equilibrium density of nuclear matter [91, 92].

The density distribution of nucleons in colliding nuclei can relax during collisions at small relative velocities, at collision energies close to the barrier. Therefore, a high nucleon density region with the density noticeably higher than the equilibrium density of nuclear matter is not formed during heavy-ion collisions leading to SHN. As a result, a realistic nucleus-nucleus potential does not show

strong repulsion at small distances between two nuclei. The behaviour of the potential at such distances is related to the sequential evolution of the shape of the nuclear system. Therefore, the nuclei can fuse and both mechanisms of compound nucleus formation, fusion and DNS, should be taken into account simultaneously in the calculation of SHN production in heavy-ion collisions. Both mechanisms of compound nucleus formation are considered briefly in Ref. [89]. Below we discuss a new model for SHN formation, which includes both mechanisms of compound nucleus formation and also the decay of the primary-formed excited compound nucleus related to neutron evaporation in competition with fission. We propose a new shape parametrization to describe the fusion path, obtain the cross section of SHN in cold fusion reactions, and compare the calculated cross section values with the experimental data.

Below we present the new model for the description of the cross section of SHN synthesis in heavy-ion collisions, which simultaneously takes into account both the fusion and DNS mechanisms of compound nucleus formation. The mechanisms of nucleus-nucleus capture and the survival of the compound nucleus applied in our model are close to the traditional ones, but we introduce some new features in the consideration of the capture and survival stages of SHN synthesis. A detailed description of our model is presented in Sec. II. The discussion of results obtained in our model for the cold fusion reactions is given in Sec. III. Conclusions are drawn in Sec. IV.

II. THE MODEL

Cold fusion reactions of SHN synthesis are related to the collisions of the projectiles nuclei ^{48}Ca, ^{50}Ti, ^{52,54}Cr, ^{58}Fe, ^{59}Co, ^{64}Ni, ^{65}Cu, and ^{70}Zn with the spherical target nuclei ^{208}Pb and ^{209}Bi [2, 5-20]. The nuclei ^{48}Ca, ^{50}Ti, and ^{70}Zn are spherical in the ground state, while the ground states of ^{52,54}Cr, ^{58}Fe, ^{59}Co, ^{64}Ni, and ^{65}Cu are weakly-deformed [94]. It is well-known that the nucleus-nucleus interaction potential depends on the nucleon density distributions and deformations of the interacting nuclei [27, 91, 92, 95-99]. The deformation of heavy nuclei affects the nucleus-nucleus potential more strongly than the deformation of light nuclei in the case of an asymmetric interacting system. Due to both the very small deformations of the projectile nuclei and the weak effect of the deformation of the light nucleus on the interaction potential, we may neglect the small deformations of the projectile nuclei in cold fusion reactions. Therefore, we can consider that spherical nuclei are participating in the cold fusion reactions.

The cross section of SHN synthesis in collisions of spherical nuclei, with the subsequent emission of x neutrons from the formed compound nucleus in competition with fission, is given as

$$\sigma^{xn}(E)=\frac{\pi\hbar^2}{2\mu E}\sum_{\ell}(2\ell+1)T(E,\ell)P(E,\ell)W^{xn}(E,\ell). \quad (1)$$

Here μ and E are the reduced mass and the collision energy, respectively, of the incident nuclei in the center of the mass system. $T(E,\ell)$ is the transmission coefficient through the fusion barrier formed by the Coulomb, centrifugal, and nuclear parts of the nucleus-nucleus interaction, $P(E,\ell)$ is the probability of compound nucleus formation, and $W^{xn}(E,\ell)$ is the survival probability of the compound nucleus related to the evaporation of x neutrons in competition with fission. In the case of cold fusion reactions, x equals 1 or 2 and rarely 3 or 4. The next subsections are devoted to a detailed description of our approach to the calculation of $T(E,\ell)$, $P(E,\ell)$, and $W^{xn}(E,\ell)$, respectively.

A. Transmission through the fusion barrier

The total potential between spherical nuclei with proton numbers Z_1 and Z_2 is

$$V_\ell(r)=\frac{Z_1Z_2e^2}{r}+V_{\rm N}^{\rm sph}(r)+\frac{\hbar^2\ell(\ell+1)}{2\mu r^2}. \quad (2)$$

Here r is the distance between the centers of mass of the nuclei, e is the charge of the proton, $V_{\rm N}^{\rm sph}(r)$ is the nuclear part of the nucleus-nucleus potential, and ℓ is the value of orbital angular momentum in $\hbar$ units.

The total interaction potential energy of two spherical nuclei can be approximated around the barrier by a parabola. The transmission coefficient through a parabolic barrier [100] is known exactly and is given by

$$T_{\rm par}(E,B_\ell^{\rm fus},\ell)=1\Big/\left[1+\exp\left(\frac{-2\pi(E-B_\ell^{\rm fus})}{\hbar\omega_\ell}\right)\right], \quad (3)$$

where $B_\ell^{\rm fus}=B_0^{\rm fus}+\dfrac{\hbar^2\ell(\ell+1)}{2\mu r_\ell^2}$ is the barrier height of the potential, r_ℓ is the barrier radius, and $\hbar\omega_\ell=\left[-\dfrac{\hbar^2}{\mu}\dfrac{{\rm d}^2V_\ell^{\rm fus}(r)}{{\rm d}r^2}\right]^{1/2}\Bigg|_{r=r_\ell}$ is the curvature of the barrier.

The fusion barrier distribution simulating a realistic multichannel coupling is often taken into account in the evaluation of sub-barrier heavy-ion fusion cross sections [101, 102] and SHN formations [51, 66, 72-74]. In this case the total transmission coefficient is given as

$$T(E,\ell)=\int_{B_1}^{B_2}{\rm d}B\,T_{\rm par}(E,B,\ell)\,f(B,B_\ell^{\rm fus}), \quad (4)$$

where $f(B,B_\ell^{\rm fus})=\dfrac{1}{g\sqrt{\pi}}\exp\left[-\left(\dfrac{B-B_\ell^{\rm fus}}{g}\right)^2\right]$ is the barrier

distribution function, which is usually approximated by a Gaussian function [51, 72-74]. The typical values of the barrier distribution width g are several MeV [51, 72-74].

In the case of sub-barrier energies $E \ll B_\ell^{\rm fus}$, Eq. (3) can be approximated in the form $T_{\rm par}(E, B_\ell^{\rm fus}, \ell) \approx \exp\left(\frac{2\pi(E-B_\ell^{\rm fus})}{\hbar\omega_\ell}\right)$. Substituting this expression into Eq. (4) and extending the limits of the integral to infinity, we get $T(E,\ell) \approx \exp\left(\frac{2\pi(E-(B_\ell^{\rm fus}-\Delta_B))}{\hbar\omega_\ell}\right)$, where $\Delta_B = \pi g^2/(2\hbar\omega_\ell)$ is the shift of the barrier value due to the barrier distribution. Using this property, we approximate the transmission coefficient through the distribution of the parabolic barriers for any values of E as

$$T(E,\ell) \approx 1\Big/\left[1+\exp\left(\frac{-2\pi(E-(B_\ell^{\rm fus}-\Delta_B))}{\hbar\omega_\ell}\right)\right]. \quad (5)$$

It is obvious that the values of $T(E,\ell)$ obtained using this formula at energies far from the barrier value are the same as those calculated with the help of Eqs. (3)-(4). The values of $T(E,\ell)$ calculated by the approximate formula (5) deviate from the exact values using Eqs. (3)-(4) at energies around the barrier. This deviation decreases with decreasing g. The application of the parameter Δ_B is simpler than a numerical integration of the barrier distribution (4) and leads to the same effect.

We should know the nucleus-nucleus potential for evaluating the transmission coefficient using Eq. (5). The nuclear part of the nucleus-nucleus potential consists of the macroscopic and the shell-correction contributions [103],

$$V_{\rm N}^{\rm sph}(r) = V_{\rm macro}(r) + V_{\rm sh}(r). \quad (6)$$

The macroscopic part $V_{\rm macro}(r)$ of the nuclear interaction of nuclei is related to the macroscopic density distribution and the nucleon-nucleon interactions of colliding nuclei. It is the Woods-Saxon form at $r > R_{\rm t}$ [103],

$$V_{\rm macro}(r) = \frac{v_1 C + v_2 C^{1/2}}{1+\exp[(r-R_{\rm t})/(d_1+d_2/C)]}. \quad (7)$$

Here $v_1 = -27.190$ MeV fm^{-1}, $v_2 = -0.93009$ MeV fm$^{-1/2}$, $d_1 = 0.78122$ fm, $d_2 = -0.20535$ fm^2, $C = R_1R_2/R_{\rm t}$ is in fm, $R_{\rm t} = R_1 + R_2$, $R_i = 1.2536A_i^{1/3} - 0.80012A_i^{-1/3} - 0.0021444/A_i$ is the radius of the i-th nucleus in fm, $i = 1, 2$, and A_i is the number of nucleons in nucleus i.

The shell-correction contribution $V_{\rm sh}(r)$ to the potential is related to the shell structure of the nuclei, which is disturbed by the nucleon-nucleon interactions of colliding nuclei. When the nuclei approach each other, the energies of the single-particle nucleon levels of each nucleus are shifted and split due to the interaction of nucleons belonging to the other nucleus. This changes the shell structures of both nuclei at small distances between them. Therefore, the shell-correction contribution to the total nuclear interaction of nuclei is introduced in Ref. [103]. This representation of the total nuclear potential energy of two nuclei is similar to the Strutinsky shell-correction prescription for the nuclear binding energy [104-107]. The shell-correction part of the potential at $r > R_{\rm t}$ is given as [103]

$$V_{\rm sh}(r) = [\delta E_1 + \delta E_2]\left[\frac{1}{1+\exp\left(\frac{R_{\rm sh}-R}{d_{\rm sh}}\right)} - 1\right], \quad (8)$$

where $R_{\rm sh} = R_{\rm t} - 0.26$ fm, $d_{\rm sh} = 0.233$ fm, and

$$\delta E_i = B_i^{\rm m} - B_i^{\rm exp} \quad (9)$$

is the phenomenological shell correction for nucleus i.

$$\begin{aligned} B_i^{\rm m} =& 15.86864A_i - 21.18164A_i^{2/3} + 6.49923A_i^{1/3} \\ &- \left[\frac{N_i - Z_i}{A_i}\right]^2 \left[26.37269A_i - 23.80118A_i^{2/3}\right. \\ &\left. - 8.62322A_i^{1/3}\right] \\ &- \frac{Z_i^2}{A_i^{1/3}}\left[0.78068 - 0.63678A_i^{-1/3}\right] - P_p - P_n \end{aligned} \quad (10)$$

is the macroscopic value of the binding energy in MeV found in the phenomenological approach, $B_{\rm exp}$ is the binding energy of the nucleus in MeV obtained using the evaluated atomic masses [108], $P_{p(n)}$ are the proton (neutron) pairing terms, which equal $P_{p(n)} = 5.62922(4.99342)$ $A_i^{-1/3}$ in the case of odd Z (N) and $P_{p(n)} = 0$ in the case of even Z_i (N_i), and N_i is the number of neutrons in nucleus i.

The parametrization of $V_{\rm N}^{\rm sph}(r_\ell)$ from Ref. [103] is used in our model, because the barrier heights $B_0^{\rm fus}$ calculated with the help of this parametrization agree well with the empirical values of barrier heights for light, medium and heavy nucleus-nucleus systems [103, 109-111]. The values of the barriers for the spherical systems ^{48}Ca, ^{48,50}Ti, ^{52}Cr, ^{54}Cr, ^{56,58}Fe, ^{64}Ni, ^{70}Zn + ^{208}Pb leading to the SHN obtained in our approach are presented in Table 1. These values of the barriers well agree with the available values of the barriers derived from an analysis of the experimental data for quasi-elastic backscattering [112]. Note that this parametrization is also successfully used for the description of the fragment mass distribution in

Table 1. The values of barrier heights between spherical nuclei $B_\ell^{\rm fus}$ for $\ell=0$, Q values of the compound nucleus formation $Q_{\rm CN}$ obtained using the evaluated atomic masses [108], the excitation energies of the compound nucleus at collision energies equal to the barrier heights $E^*_{\rm bar}=E+Q_{\rm CN}$, and the available values of the barrier heights $B_{\rm qebs}$ derived from an analysis of the experimental data for quasi-elastic backscattering [112]. All values are given in MeV.

Collision systems	$B_0^{\rm fus}$	$-Q_{\rm CN}$	$E^*_{\rm bar}$	$B_{\rm qebs}$
^{48}Ca + ^{208}Pb	172.5	153.8	18.7	
^{48}Ti + ^{208}Pb	191.0	164.5	26.5	190.1
^{50}Ti + ^{208}Pb	189.8	169.5	20.3	
^{52}Cr + ^{208}Pb	207.2	183.7	23.5	
^{54}Cr + ^{208}Pb	206.0	187.1	19.0	205.8
^{56}Fe + ^{208}Pb	223.2	201.9	21.3	223.0
^{58}Fe + ^{208}Pb	222.0	205.0	17.0	
^{64}Ni + ^{208}Pb	236.6	224.9	11.9	236.0
^{70}Zn + ^{208}Pb	251.1	244.2	6.9	250.6

the fission of highly-excited nuclei [97, 98] and in ternary fission [99]. So, the values of the barrier heights obtained in our approach are reliable.

Using Eqs. (2), (5)-(10) we can evaluate the capture cross section,

$$\sigma_{\rm cap}(E)=\frac{\pi\hbar^2}{2\mu E}\sum_\ell(2l+1)T(E,\ell). \tag{11}$$

The capture cross section is related to the fusion barrier penetration. The capture cross section coincides with the compound nucleus production cross section in the case of collisions of light and medium nuclei, where the decay of the DNS to fragments and the quasi-fission process give negligible contributions [101, 102, 111, 113, 114]. In the case of collisions of heavy nuclei, the capture cross section is linked to the formation of the DNS.

B. Probability of compound nucleus formation

1. *Expression for the probability of compound nucleus formation*

The fusion barrier between incident spherical nuclei is high. The collision energy of the two nuclei starts to dissipate just before the barrier. After passing the incident fusion barrier the nuclei are located in the capture well, which is close to the contact distance of the nuclei. The nuclei form the DNS in the capture well. The DNS formed in the capture well is the injection point for subsequent stages of SHN formation and DNS evolution.

The kinetic energy related to the relative motion of the colliding nuclei is quickly dissipated at the initial collision stage, when the tails of nucleon densities of the nuclei start to overlap. As a result, the kinetic energy of the relative motion of nuclei transfers into the intrinsic energy of the DNS [90, 115]. Therefore, the subsequent stages of SHN synthesis can be considered in the framework of the statistical approach. In this approach the probability of compound nucleus formation is linked to the ratio of the decay widths of different processes. The widths considered in this subsection are defined in the framework of the Bohr-Wheeler transition state statistical approach [116].

The DNS formed in the capture well may decay into different channels such as, for example, spherical or deformed incident nuclei, new DNSs formed at the transfer of nucleons between the incident nuclei, and formation of a compound nucleus. Due to the transfer of nucleons between nuclei the DNS may decay into more symmetric nucleus-nucleus systems with subsequent decay to deformed nuclei, or into more asymmetric nucleus-nucleus systems with subsequent formation of a compound nucleus. The DNS may also decay into a compound nucleus by smooth shape evolution. The corresponding decay branches of the DNS are linked to the respective decay widths and barriers.

The probability of a specific decay process is related to the passing through the barrier in competition with other processes. The compound nucleus is formed by passing the barrier in fusion, and the DNS barrier is related to the transfer of nucleons from the light nucleus to the heavy one. Passing through other barriers is linked to the decay of the DNS to scattered nuclei.

Therefore, the probability of compound nucleus formation from the DNS is determined in our model as the ratio of the widths leading to the compound nucleus to the total decay widths of the DNS, i.e.:

$$P(E,\ell)=\frac{\Gamma_{\rm CN}^{\rm DNS,f}(E,\ell)+\Gamma_{\rm CN}^{\rm DNS,tr}(E,\ell)}{\Gamma_{\rm CN}^{\rm tot}(E,\ell)}. \tag{12}$$

Here,

$$\begin{aligned}\Gamma_{\rm CN}^{\rm tot}(E,\ell)=&\Gamma_{\rm CN}^{\rm DNS,f}(E,\ell)+\Gamma_{\rm CN}^{\rm DNS,tr}(E,\ell)+\Gamma_{\rm DIC}^{\rm DNS}(E,\ell)\\&+\Gamma_{\rm sph}^{\rm DNS}(E,\ell)+\Gamma_{\rm def}^{\rm DNS}(E,\ell)\end{aligned} \tag{13}$$

is the total decay width of the DNS. $\Gamma_{\rm CN}^{\rm DNS,f}(E,\ell)$ is the width related to compound nucleus formation through the fusion path by the smooth evolution of shape of the nuclear system. $\Gamma_{\rm CN}^{\rm DNS,tr}(E,\ell)$ is the width of the compound nucleus production through multi-nucleon transfer from the light to heavy nuclei. This is the DNS path of compound nucleus formation used in the various versions of the DNS model [60-75, 78]. $\Gamma_{\rm DIC}^{\rm DNS}(E,\ell)$ is the width of the DNS decay into two nuclei with nucleon transfer from heavy to light nuclei. During this process the DNS de-

cays into scattered nuclei, which are close to the incident nuclei. This is the deep-inelastic collision (DIC) process. $\Gamma^{\rm DNS}_{\rm sph}(E,\ell)$ and $\Gamma^{\rm DNS}_{\rm def}(E,\ell)$ are the width of the DNS decay into incident spherical or deformed nuclei, respectively. The widths $\Gamma^{\rm DNS}_{\rm sph}(E,\ell)$ and $\Gamma^{\rm DNS}_{\rm def}(E,\ell)$ are connected to the different quasi-elastic decay modes of the DNS.

Equation (12) is written for the case of a direct coupling of the DNS to the equilibrium shape of the compound nucleus. In this case the potential energy landscape has a valley, the bottom of which directly connects the system of contacting nuclei and the equilibrium shape of the compound nucleus. This is seen, for example, in the landscapes presented in Fig. 1. If the final point of the valley starting from the DNS is related to the non-equilibrium shape of the compound nucleus and the equilibrium shape of the compound nucleus is located in another valley, as seen, for example, in the landscapes presented in Fig. 2, then an intermediate state should be introduced. The intermediate state can decay into both the compound nucleus in equilibrium shape and to quasi-fission fragments. Such cases of compound nucleus formation will be considered in Sec. IIB.3.

According to Eqs. (12)-(13), the compound nucleus in our model can be formed by both the fusion and DNS paths. If we put $\Gamma^{\rm DNS,f}_{\rm CN}(E,\ell)=0$ and introduce $\Gamma_{\rm quasi-fission}(E,\ell)=\Gamma^{\rm DNS}_{\rm DIC}(E,\ell)+\Gamma^{\rm DNS}_{\rm sph}(E,\ell)+\Gamma^{\rm DNS}_{\rm def}(E,\ell)$, then our probability of compound nucleus formation (12)-(13) equals that in Refs. [59-62]. Here we use the original name of the width $\Gamma_{\rm quasi-fission}(E,\ell)$ used in Refs. [59-62]. Note that in our model the quasi-fission process is related to the decay of the one-body nuclear shape to the fission fragments, bypassing the formation of the compound nucleus with the equilibrium shape. (Recently, the authors of the DNS model have used the master equation approach to evaluate the probability of compound nucleus formation [65-70, 72-75]. However, the old [59-62] and new [65-70, 72-75] approaches of the DNS model have the same mechanism of compound nucleus formation. In our model the probability of compound nucleus formation is described by the ratio of the decay widths in Eqs. (12)-(13). This is very convenient, because all decay processes are considered in the same approach.)

The shape and properties of the potential energy landscape related to the fusion trajectory of compound nucleus formation is discussed in the next subsection.

2. *Landscape of potential energy related to the fusion path from DNS to compound nucleus*

The DNS is formed in the collision of two spherical nuclei in the case of cold fusion reactions. The DNS after formation can evolve to a compound nucleus or divide into two spherical or deformed nuclei. The division of the DNS into two deformed fragments can be linked to quasi-fission as well as to the immediate decay of the DNS.

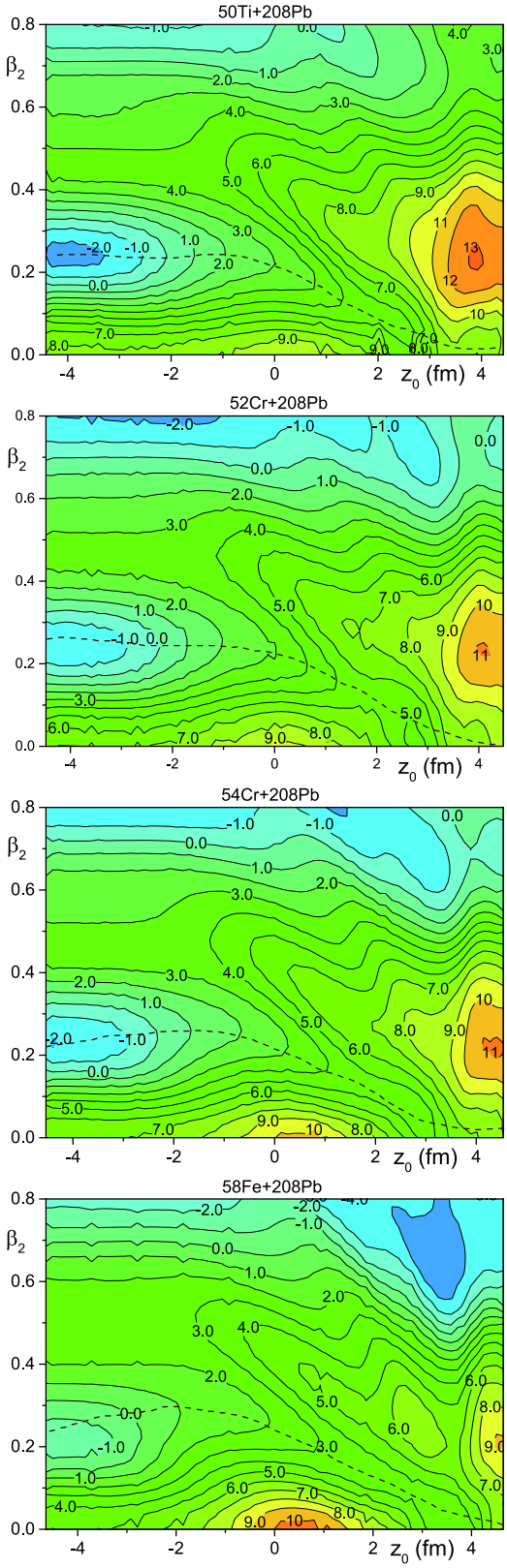

Fig. 1. (color online) The potential energy landscape as a function of the variables z_0 and β_2 for the cold-fusion systems ^{50}Ti, ^{52,54}Cr, and ^{58}Fe + ^{208}Pb. The dashed lines are the trajectories of compound nucleus formation, which are drawn by eye.

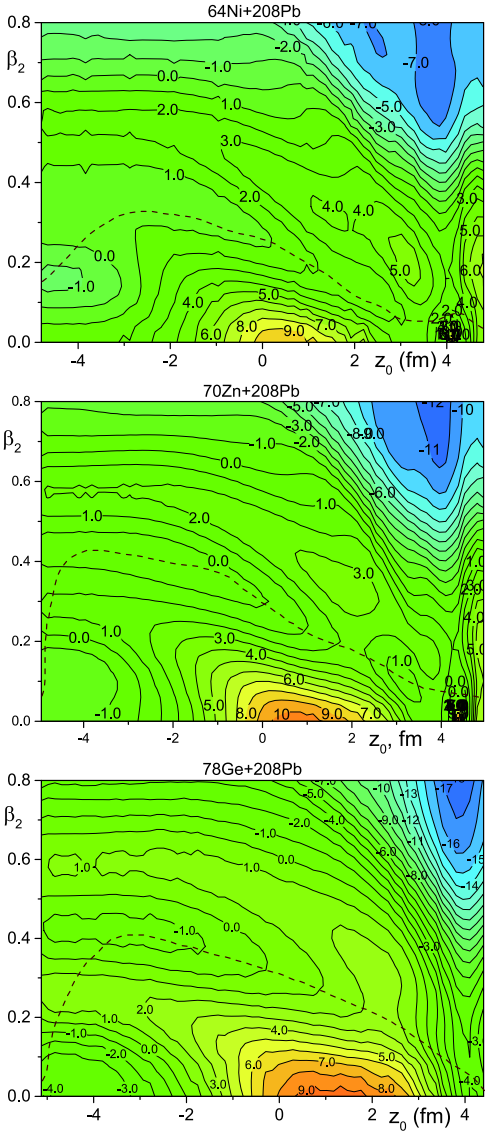

Fig. 2. (color online) The potential energy landscape as a function of the variables z_0 and β_2 for the cold-fusion systems ^{64}Ni, ^{70}Zn, and ^{78}Zn + ^{208}Pb. The dashed lines are the compound nucleus formation trajectories, which are drawn by eye.

Therefore, the shapes of nuclei related to the analysis of the trajectory from the DNS to the compound nucleus, with the possibility of quasi-fission, should include the two spherical or deformed nuclei as well as the spherical, well-deformed, and pre-ruptured one-body nuclear shapes. The parametrization describing such different shapes should be as simple as possible. The axial-symmetric parametrization,

$$\rho = \begin{cases} 0, & \text{if } z < -a, \\ b\sqrt{1-(z/a)^2}, & \text{if } -a \leqslant z \leqslant z_0, \\ c\sqrt{1-((z-R)/d)^2}, & \text{if } z_0 \leqslant z \leqslant R+d, \\ 0, & \text{if } z > R+d \end{cases} \tag{14}$$

satisfies the proposed conditions. Here ρ and z are cylindrical coordinates. The parametrization depends on the 6 parameters a, b, c, d, z_0, and R.

The radius ρ should be continued at point z_0, therefore

$$b\sqrt{1-(z_0/a)^2} = c\sqrt{1-((z_0-R)/d)^2}. \tag{15}$$

This equation couples the two parameters of the parametrization, for example, z_0 and R. The total volume of the nuclear system should be conserved during the shape evolution of the nuclear system. As a result of these constraints, the shape parametrization has 4 independent parameters.

We fix the values $a = b = R_1$, where R_1 is the radius of the light incident nucleus. Due to this fixing the shape parametrization (14) depends only on two independent parameters. Note that two independent parameters are often used to describe compound nucleus formation in the evolution of the one-body form; see, for example, Refs. [43, 47, 57, 58, 89].

The two touching nuclei are described by Eq. (14) at $z_0 = R_1$. During fusion the nuclei get close and the value of z_0 is smoothly reduced. The radius of the neck connecting the nuclei rises from 0 at $z_0 = R_1$ up to the radius of the light nucleus R_1 at $z_0 = 0$. After that the heavy nucleus absorbs the light one and z_0 approaches $-R_1$. The light nucleus is fully absorbed by the heavy one at $z_0 = -R_1$.

It is useful to consider two independent variables z_0 and β_2 to specify the shape of the fusing nuclei. Parameter β_2 is coupled to the ratio d/c by the equation $d/c = [1+\beta_2 Y_{20}(\theta = 0°)]/[1+\beta_2 Y_{20}(\theta = 90°)]$, where $Y_{20}(\theta)$ is the spherical harmonic function [117]. Parameter β_2t describes the quadrupole deformation of the heavy nucleus in the case of the touching nuclei at $z_0 = R_1$, or the quadrupole deformation of the one-body shape at $z_0 = -R_1$. (Here we neglect the difference between the equal-volume shapes of the axial-symmetric ellipsoid and the nucleus with the surface radius $R(\theta) = R_0[1+\beta_2 Y_{20}(\theta)]$. Such shapes are very close to each other at small deformations.) Our shape parametrization at $z_0 = -R_1$ also describes the fission process related to the evolution of the quadrupole deformation. Note that the quadrupole deformation is successfully used for a discussion of the fission process by Bohr and Wheeler [116].

Our two-parameter parametrization is useful for the simultaneous description of various nuclear shapes related to the fusion of asymmetric nuclei, compound nucleus formation, fission and quasi-fission. This parametrization has not previously been used anywhere; see, for example, Ref. [118], which is devoted to the compilation of various nuclear shapes used in the literature.

For every value z_0 and β_2 we find parameters R^{fit} and

β_L^{fit}, at which the parametrization

$$R(\theta) = R^{fit}\left[1 + \sum_{L=2}^{9}\beta_L^{fit}Y_{L0}(\theta)\right] \quad (16)$$

fits the shape described by Eq. (14). Using the obtained values of parameters R^{fit} and β_L^{fit}, we calculate the shell correction energies as a function of the parameters z_0 and β_2 by using the code WSBETA [119]. This code uses a Woods-Saxon potential with a 'universal' parameter set and a parametrization of the nuclear shape in the form $R(\theta) \propto [1 + \sum_{L=2}^{9}\beta_L^{fit}Y_{L0}(\theta)]$. The radius parameter of the Woods-Saxon potential is fixed by the 'universal' parameter set [119]. Therefore, the parameters z_0 and β_2 are coupled to the deformation parameters β_L^{fit} only. The residual pairing interaction is calculated by means of the Lipkin-Nogami method [120]. The macroscopic part of the deformation energy is evaluated using the Yukawa-plus-exponential potential [121].

The dependencies of the potential energy landscape on the variables z_0 and β_2 for the cold-fusion systems ^{50}Ti, ^{52,54}Cr, ^{58}Fe, ^{64}Ni, ^{70}Zn, and ^{78}Ge + ^{208}Pb are presented in Figs. 1-2. The dependencies of the potential energy of nuclei on β_2 at $z_0 = -R_1$ presented in these figures are typical for fissioning nuclei. So, we see the ground-state well and the fission barrier along the line $z_0 = -R_1$ in these figures.

There are many heavy and super-heavy nuclei with the two-hampered fission barrier [122, 123, 124-138]. The values of β_2 for the ground state of the compound nucleus, which we can see in Figs. 1-2 at $z_0 \approx -R_1$, are close to the corresponding ones obtained in Ref. [124]. The values of the inner fission barrier evaluated from Figs. 1-2 at $z_0 \approx -R_1$t are close to those obtained in Refs. [124, 127, 132, 135, 136] in the framework of the shell-correction approach. Note that Refs. [122, 123, 124, 132, 135, 136] are devoted to accurate calculations of the ground state and saddle point properties of SHN using a rich set of the multipole deformations. Our deformation space is limited by two independent variables, therefore the agreement of the fission barrier values extracted from Figs. 1-2 with the results obtained in the framework of other models is approximate.

The dependence of the potential energy of two contacting nuclei on the value of quadrupole deformation of the heavy nucleus is presented in Figs. 2-3 at $z_0 = R_1$. We see that the potential energy has a local minimum at small values of $\beta_2 \approx 0$ at $z_0 = R_1$, which is related to the spherical ground-state shape of ^{208}Pb. Note that the similarity of the shapes described by the parametrizations (14) and (16) worsens as $z_0 \to R_1$. Nevertheless, the shape described by Eq. (16) is close to the shape of the two contacting nuclei.

The landscape of potential energy is strongly changed near $z_0 = R_1$ for the system ^{78}Ge + ^{208}Pb. As a result, the contour lines are difficult to separate. We therefore present the potential landscape for this system for $z_0 \leqslant 4.4$ fm, see Fig. 2.

The trajectory of the compound nucleus formation, which is drawn by eye in Figs. 1-2, connects the point of the two contacting spherical nuclei at $z_0 = R_1, \beta_2 = 0$ and the point of the ground state of the compound nucleus at $z_0 \approx -R_1$ and β_2 in the range $0 \leqslant \beta_2 \leqslant 0.25$. These trajectories for the cold-fusion systems ^{50}Ti, ^{52,54}Cr, ^{58}Fe + ^{208}Pb are located in the bottom of the valley leading to compound nucleus formation, see Fig. 1. Similar valleys are also obtained for cluster emission from heavy nuclei with the daughter nucleus near ^{208}Pb in Ref. [139]. The fusion path leading to compound nucleus formation is also studied in Refs. [140, 141]. The dependencies of the potential energies on the elongation along the fusion paths presented in Refs. [140, 141] for reactions ^{50}Ti and ^{70}Zn + ^{208}Pb look like the ones in Figs. 1 and 2 for these systems. Unfortunately, direct comparison of the potentials along the fusion trajectories obtained in these different approaches is not possible due to the use of different shape parametrizations.

The high ridge separates the fusion valley and the quasi-fission area in Fig. 2. This ridge merges smoothly with the inner fission barrier at $z_0 = -R_1$. The true quasi-fission (or fast fission) process in heavy-ion reactions is related to the fission of the nuclear system before it reaches the ground-state shape of the compound nucleus, while true fission starts from the ground-state shape of the compound nucleus. The large difference between the energies at the bottom of the fusion valley and at the ridge leads to a statistical suppression of the quasi-fission process compared to compound nucleus formation for the systems ^{50}Ti, ^{52,54}Cr, ^{58}Fe + ^{208}Pb. Therefore, the probabilities of compound nucleus formation are well determined by Eqs. (12)-(13) for these systems.

We see the saddle points at the point $z_0 \approx 2-4$ fm and $\beta_2 \approx 0.1-0.25$ on the fusion path for systems ^{64}Ni, ^{70}Zn, and ^{78}Ge + ^{208}Pb in Fig. 2. The heights of these saddle points define the barriers for the transition from the DNS to the compound nucleus along the fusion trajectories for these systems. In contrast to this, such saddle points are absent from the fusion paths for reactions ^{50}Ti, ^{52,54}Cr, and ^{58}Fe + ^{208}Pb in Fig. 1. Therefore, the barriers related to the formation of the compound nucleus along the fusion trajectory for reactions ^{50}Ti, ^{52,54}Cr, and ^{58}Fe + ^{208}Pb are defined as the highest values of the potential energies of spherical or near-spherical nuclei at the contact point, see Fig. 1. This is because the excitation energies of these systems at the contact point should be above or equal these potential energies for successful formation of the compound nuclei.

The trajectories of compound nucleus formation for

the reactions ^{64}Ni, ^{70}Zn, and ^{78}Ge + ^{208}Pb have saddle points near the point $z_0 \approx 4$ fm and $\beta_2 \approx 0.1-0.2$, which are linked to the decay of the slightly overlapped nuclei (or the DNS) to two fragments, see Fig. 2. The decay of the DNS to two fragments is also described by the widths $\Gamma^{\rm DNS}_{\rm DIC}(E,\ell)$, $\Gamma^{\rm DNS}_{\rm sph}(E,\ell)$ and $\Gamma^{\rm DNS}_{\rm def}(E,\ell)$. The width $\Gamma^{\rm DNS}_{\rm def}(E,\ell)$ is connected to the lowest value of the barrier, which takes place for two-body systems. The height of the saddle point near the point $z_0 \approx 4$ fm and $\beta_2 \approx 0.1-0.2$ is higher than the barrier related to the width $\Gamma^{\rm DNS}_{\rm def}(E,\ell)$. Therefore, we may neglect the influence of this saddle point on both the formation of the compound nucleus and the decay of the DNS to fragments.

The ridge, which separates the compound nucleus formation valley and the quasi-fission valley, merges with the outer fission barrier near $z_0 \approx -R_1$ for the cold-fusion systems ^{70}Zn and ^{78}Ge + ^{208}Pb, see Fig. 2. The compound nucleus formation valley is merged with the potential energy well between the inner and outer fission barrier near $z_0 \approx -R_1$. Therefore, an intermediate state is formed in this well. The compound nucleus is formed at the decay of the intermediate state through the inner fission barrier. The quasi-fission fragments can appear in the decay of the intermediate state through the outer fission barrier. The quasi-fission fragments are different from those produced in the decay of the DNS to two fragments and are related to the DIC or quasi-elastic processes. This is because the yield of the DIC or quasi-elastic fragments is concentrated around the incident nuclei, while the yield of the quasi-fission fragments is similar to that for the compound nucleus fission.

The probabilities of compound nucleus formation for the systems ^{70}Zn, and ^{78}Ge + ^{208}Pb are not described by Eqs. (12)-(13), because we should take into account the decay branches of the intermediate state. We consider the probability of compound nucleus formation in such a case in the next subsection.

3. *Expression for the probability of compound nucleus formation in the case of an intermediate state*

The formation of a compound nucleus in the case of an intermediate state occurs in two steps. The first step is related to the formation of the intermediate state from the DNS, while the second is linked to the decay of the intermediate state into the compound nucleus with the equilibrium shape. The intermediate state may decay into the compound nucleus, into quasi-fission fragments, or back to the DNS.

The consideration of the two-step process in the model is similar to the discussion of the sequential stages of SHN formation used in Eq. (1). The intermediate state takes place on the fusion path of the compound nucleus formation and has no influence on the DNS path of the compound nucleus formation. As a result, the probability of compound nucleus formation in this case is determined as

$$P(E,\ell) = \frac{\Gamma^{\rm DNS,f}_{\rm CN}(E,\ell)P_{\rm is}(E,\ell) + \Gamma^{\rm DNS}_{\rm CN}(E,\ell)}{\Gamma^{\rm tot}_{\rm CN}(E,\ell)}, \qquad (17)$$

where

$$P_{\rm is}(E,\ell) = \frac{\Gamma^{\rm is}_{\rm CN}(E,\ell)}{\Gamma^{\rm is}_{\rm tot}(E,\ell)} \qquad (18)$$

is the decay probability of the intermediate state into the compound nucleus. The widths presented in Eq. (17) have been discussed already, see Eqs. (12)-(13). Now we consider the widths which appear in Eq. (18).

$$\Gamma^{\rm is}_{\rm tot}(E,\ell) = \Gamma^{\rm is}_{\rm CN}(E,\ell) + \Gamma^{\rm is}_{\rm qf}(E,\ell) + \Gamma^{\rm is}_{\rm DNS}(E,\ell) \qquad (19)$$

is the total decay width of the intermediate state, $\Gamma^{\rm is}_{\rm CN}(E,\ell)$, $\Gamma_{\rm fiss}(E,\ell)$, and $\Gamma^{\rm is}_{\rm DNS}(E,\ell)$ are the decay widths of the intermediate state to the compound nucleus, the quasi-fission fragments, and the DNS, respectively. The width $\Gamma_{\rm qf}(E,\ell)$ describes the true quasi-fission process, which is related to the fission of the one-body nuclear system, bypassing the formation of a compound nucleus with equilibrium shape.

The probability of compound nucleus formation decreases due to the decay of the intermediate state to the quasi-fission fragments or back to the DNS, because $P_{\rm is}(E,\ell) \leqslant 1$. Eq. (17) coincides with Eq. (12), when $P_{\rm is}(E,\ell) = 1$.

The cross sections of compound nucleus formation and true quasi-fission are related to the corresponding decay branches of the intermediate state. Therefore, these cross sections can be defined, respectively, as:

$$\sigma_{\rm CN}(E) = \frac{\pi\hbar^2}{2\mu E}\sum_{\ell}(2l+1)T(E,\ell)P(E,\ell), \qquad (20)$$

$$\sigma_{\rm qf}(E) = \frac{\pi\hbar^2}{2\mu E}\sum_{\ell}(2l+1)T(E,\ell)P_{\rm qf}(E,\ell). \qquad (21)$$

Here,

$$P_{\rm qf}(E,\ell) = \frac{\Gamma^{\rm DNS,f}_{\rm CN}(E,\ell)}{\Gamma^{\rm tot}_{\rm CN}(E,\ell)} \times \frac{\Gamma^{\rm is}_{\rm qf}(E,\ell)}{\Gamma^{\rm is}_{\rm tot}(E,\ell))} \qquad (22)$$

is the probability of the quasi-fission decay. The first factor in Eq. (22) is the probability of intermediate state formation, while the second is the decay probability of the intermediate state to quasi-fission fragments.

The number of successive intermediate states k may be more than one in the case of a very complex potential energy landscape. In such cases the probability of compound nucleus formation is also determined by Eq. (17), in which the probability $P_{\rm is}(E,\ell)$ is substituted by the product of the decay probabilities of k successive intermediate states $P_{{\rm is}\,1}(E,\ell)\cdot P_{{\rm is}\,2}(E,\ell)\cdot\ldots\cdot P_{{\rm is}\,k}(E,\ell)$. Equations (21)-(22) for the quasi-fission cross section should be also modified similarly, because the quasi-fission fragments can be emitted in the decay of any intermediate state. The total number of corresponding parameters, which is needed to describe the reaction, rises with the number of intermediate states. Therefore, in our model we consider only one intermediate state for the reactions ^{70}Zn and ^{78}Ge + ^{208}Pb.

The main decay channel of the superheavy compound nucleus is fission. Consequently, the values of the compound nucleus production cross sections are very close to the compound nucleus fission cross sections. The probabilities of formation of compound nucleus fission fragments (12), (13) or quasi-fission fragments (22) are very small for heavy cold-fusion systems. Therefore, the probabilities of these processes are much lower than the probability of DIC fragments being formed in the DNS decay, because it is necessary to form a compound nucleus or intermediate state as well as the DNS. This is strongly correlated to the experimental yields of near-symmetric fission or quasi-fission fragments and very asymmetric DIC or quasi-elastic fragments for various reactions [34, 142-144].

4. *Decay widths*

Equations (12)-(13), (17)-(19), and (22) include two types of widths. The widths $\Gamma_{\rm CN}^{\rm DNS,f}(E,\ell)$, $\Gamma_{\rm CN}^{\rm is}(E,\ell)$, $\Gamma_{\rm qf}^{\rm is}(E,\ell)$, $\Gamma_{\rm DNS}^{\rm is}(E,\ell)$ are related to the one-body shape of the nucleus, while the widths $\Gamma_{\rm CN}^{\rm DNStr}(E,\ell)$, $\Gamma_{\rm DIC}^{\rm DNS}(E,\ell)$, $\Gamma_{\rm sph}^{\rm DNS}(E,\ell)$, $\Gamma_{\rm def}^{\rm DNS}(E,\ell)$ are linked to two-body nuclear systems.

The widths linked to the various one-body shapes are determined as

$$\Gamma_{\rm one-body}(E,\ell)=\frac{1}{\rho_{\rm in}(E)}\int_0^{E-B}{\rm d}\varepsilon\,\rho_{A,\ell}(\varepsilon). \tag{23}$$

Here $\rho_{\rm in}(E)$ is the energy level density of the nuclear system in the initial state, $\rho_{A,\ell}(\varepsilon)$ is the energy level density of the nuclear system in the final state, B is the height of the saddle point on the way from the initial state to the final one, and ε is the excitation energy. The corresponding values of E, ℓ and B should be applied in the calculation of the widths $\Gamma_{\rm CN}^{\rm DNS,f}(E,\ell)$, $\Gamma_{\rm CN}^{\rm is}(E,\ell)$, $\Gamma_{\rm qf}^{\rm is}(E,\ell)$, $\Gamma_{\rm DNS}^{\rm is}(E,\ell)$.

We use the back-shifted Fermi gas energy level density of the nucleus with the excitation energy ε, A nucleons and the angular momentum J [145], which is written as

$$\rho_{A,J}(U)=\frac{(2J+1)}{4\sqrt{2\pi}\sigma_J^3}\exp\left\{-[(J+1/2)/\sigma_J]^2/2\right\}\times\frac{\sqrt{\pi}}{12(a_{\rm dens}U^5)^{1/4}}\exp\left[2\sqrt{a_{\rm dens}U}\right]. \tag{24}$$

Here,

$$U=\varepsilon-\delta=a_{\rm dens}T^2 \tag{25}$$

is the back-shifted excitation energy, which is connected with the temperature T,

$$\delta=12nA^{-1/2}+0.173015 \tag{26}$$

is the energy shift with $n=-1,0$ and 1 for odd-odd, odd-A, and even-even nuclei, respectively, $\sigma_J^2=(0.83A^{0.26})^2$ is the spin cut-off parameter. The level density parameter depends on the excitation energy of the nucleus [146] and equals

$$a_{\rm dens}=a_{\rm inf}[1+(\delta_{\rm shell}/U)(1-\exp(-\gamma U))], \tag{27}$$

where

$$a_{\rm inf}=0.0722396A+0.195267A^{2/3} \tag{28}$$

is the asymptotic level density parameter, $\gamma=0.410289/A^{1/3}$ is the damping parameter, and $\delta_{\rm shell}$ is the phenomenological shell correction [145]. The value of the phenomenological shell correction is determined as the difference $\delta_{\rm shell}=M_{\rm exp}-M_{\rm ld}$ [145], where $M_{\rm exp}$ is the experimental value of the nuclear mass taken from Ref. [108] and $M_{\rm ld}$ is the liquid drop component of the mass formula [147]. All parameter values used for the evaluation of the energy level density are taken from Ref. [145] without any changes. (Note that the phenomenological shell corrections $\delta_{\rm shell}$ and δE_i, see Eq. (9), have the same physical sense. However, they are obtained using different mass formulas for the calculation of the liquid-drop contribution [103, 145, 147]. The values of the parameters $\delta_{\rm shell}$ and δE_i are, respectively, linked to the values of other parameters of the energy level density and the nuclear part of the interaction potential. Therefore, we use different expressions for the calculations of $\delta_{\rm shell}$ and δE_i.) The values of the shell corrections are very important for the properties of SHN [148], and therefore the influence of shell correction on the level density should be taken into account.

As we have pointed out, the widths $\Gamma_{\rm CN}^{\rm DNS,tr}(E,\ell)$, $\Gamma_{\rm DIC}^{\rm DNS}(E,\ell)$, $\Gamma_{\rm sph}^{\rm DNS}(E,\ell)$, $\Gamma_{\rm def}^{\rm DNS}(E,\ell)$ are related to the DNS,

which consists of two nuclei with various shapes and nucleon compositions. The width of the DNS built by nuclei with numbers of nucleons A_1 and $A_2 = A - A_1$, correspondingly, is written as

$$\Gamma_{\rm DNS}(E,\ell) = \frac{1}{\rho_{\rm in}(E)} \int_0^{E-B_\ell} {\rm d}\varepsilon\, \rho_{A_1,A_2}(\varepsilon,\ell), \tag{29}$$

where

$$\rho_{A_1,A_2}(\varepsilon,\ell) = \int_0^{\varepsilon} {\rm d}\varepsilon'\, \rho_{A_1,0}(\varepsilon')\, \rho_{A_2,0}(\varepsilon-\varepsilon'). \tag{30}$$

Here $\rho_{\rm in}(E)$ is the energy level density of the nuclear system in the initial state. $\rho_{A_1,A_2}(\varepsilon,\ell)$ is the energy level density of the DNS, $\rho_{A_1,\ell}(\varepsilon)$ and $\rho_{A_2,\ell}(\varepsilon)$ are the energy level density of the nuclei with A_1 and A_2 nucleons in the final state, and B_ℓ is the height of the saddle point on the way from the initial state to the final one. We neglect the transfer of the orbital moment of the DNS system into the orbital momenta of the nuclei for the sake of simplicity.

The probabilities of the compound nucleus formation $P(E,\ell)$ and the decay of the intermediate state $P_{\rm is}(E,\ell)$ depend on the ratio of the decay widths into specific states to the total decay width of the initial state. Therefore, these probabilities are independent of $\rho_{\rm in}(E)$.

We should define the barrier heights for the calculation of various decay widths and the probabilities. Let us consider the barriers for corresponding widths in detail.

5. *Barrier heights for different processes*

The width $\Gamma^{\rm DNS}_{\rm sph}(E,\ell)$ depends on the barrier $B^{\rm fus}_\ell$. The value of $B^{\rm fus}_\ell$ is obtained in the calculation of the transmission probability $T(E,\ell)$, see Eq. (5). This barrier of the total potential energy of the spherical incident nuclei can be found using Eqs. (2), (6)-(10). Substituting the value of $B^{\rm fus}_\ell$ into Eq. (29), we obtain $\Gamma^{\rm DNS}_{\rm sph}(E,\ell)$.

The width $\Gamma^{\rm DNS}_{\rm def}(E,\ell)$ is connected to the barrier $B^{\rm fus}_{\ell,{\rm def}}$. This barrier is determined as the minimal values of the barrier of the total potential energy of the deformed nuclei. The nucleon compositions of these deformed nuclei are the same as in the incident channel. The total potential energy of the deformed nuclei is calculated in the framework of the approach developed in Refs. [97-99]. Now we improve it by taking into account a realistic surface stiffness for the interacting nuclei.

As shown in Refs. [27, 95, 96, 149-152], axially-symmetric nuclei, which are elongated along the line connecting the mass centers, have the lowest value of the barrier height. Therefore, we consider that the DNS decays preferentially by such mutual orientation of the axially-symmetric nuclei. The other nucleus-nucleus configurations have higher values of the barrier. Consequently, such configurations have lower values of the thermal excitation energy of the DNS and smaller values of the statistical yield. As a result, such configurations may be neglected.

The total potential energy of interacting deformed nuclei, $V_{\rm DNS}(r,\ell,\{\beta_{L1}\},\{\beta_{L2}\})$, consists of the nuclear $V_{\rm N}(R,\{\beta_{L1}\},\{\beta_{L2}\})$, Coulomb $V_{\rm C}(R,\{\beta_{L1}\},\{\beta_{L2}\})$, and centrifugal $V_\ell(R,\{\beta_{L1}\},\{\beta_{L2}\})$ energies as well as the deformation energies $E_{{\rm def}i}(\{\beta_{Li}\})$ of each nucleus. So, the total potential energy equals

$$\begin{aligned} V_{\rm DNS}(r,\ell,\{\beta_{L1}\},\{\beta_{L2}\}) =& V_{\rm N}(r,\{\beta_{L1}\},\{\beta_{L2}\}) \\ &+V_{\rm C}(r,\{\beta_{L1}\},\{\beta_{L2}\})+V_\ell(r,\{\beta_{L1}\},\{\beta_{L2}\}) \\ &+E_{\rm def1}(\{\beta_{L1}\})+E_{\rm def2}(\{\beta_{L2}\}), \end{aligned} \tag{31}$$

where $\{\beta_{Li}\} = \beta_{0i},\beta_{1i},\beta_{2i},\beta_{3i},\beta_{4i}$ is the set of surface multipole deformation parameters of nucleus i, $i = 1,2$. These deformation parameters are related to the surface radius of the deformed nucleus,

$$R_i(\theta) = R_{0i}\left[1 + \sum_L \beta_{Li} Y_{L0}(\theta)\right], \tag{32}$$

where R_{0i} is the radius of spherical nucleus i and $Y_{L0}(\theta)$ is the spherical harmonic function [117]. The parameters β_{0i} and β_{1i} provide the volume conservation and non-movement of the position of the mass center for nucleus i. The values of the deformation parameters $\{\beta_{L1}\},\{\beta_{L2}\}$ are determined by the condition of the minima of the total interaction potential energy of these nuclei $V_{\rm DNS}(r,\ell,\{\beta_{L1}\},\{\beta_{L2}\})$ at given r. Note that the contributions of higher multipole deformations $\beta_{L\geqslant 5}$ to the value of $V_{\rm DNS}(r,\ell,\{\beta_{L1}\},\{\beta_{L2}\})$ are negligible.

According to the proximity theorem [153, 154], the nuclear part of the interaction potential between deformed nuclei can be approximated as [97, 98]

$$\begin{aligned} V_{\rm N}(r,\{\beta_{L1}\},\{\beta_{L2}\}) \approx& S(\{\beta_{L1}\},\{\beta_{L2}\}) \\ &\times V^{\rm sph}_{\rm N}(d(r,\{\beta_{L1}\},\{\beta_{L2}\})+R_{01}+R_{02}). \end{aligned} \tag{33}$$

Here,

$$S(\{\beta_{L1}\},\{\beta_{L2}\}) = \frac{R_1(\pi/2)^2 R_2(\pi/2)^2}{R_1(\pi/2)^2 R_2(0)+R_2(\pi/2)^2 R_1(0)} \Big/ \frac{R_{01}R_{02}}{R_{01}+R_{02}} \tag{34}$$

is the factor related to the modification of the strength of nuclear interaction of the deformed nuclei induced by the surface deformations, which is derived in Ref. [97], and

$$\mathrm{d}(r,\{\beta_{L1}\},\{\beta_{L2}\}) = r - R_1(0) - R_2(0) \tag{35}$$

is the smallest distance between the surfaces of the deformed nuclei, which coincides with the distance between the surfaces of spherical nuclei. The potential $V_{\rm N}^{\rm sph}$ determines the nuclear part of the interaction between spherical nuclei, see Eqs. (6)-(10).

The expression for the Coulomb interaction of the two deformed arbitrarily-oriented axial-symmetric nuclei is obtained by an expansion of the deformation parameters in Ref. [95]. The accuracy of this expression is very high. The values of the Coulomb interaction of two deformed arbitrarily-oriented axial-symmetric nuclei evaluated by using the expression from Ref. [95] and by numerical calculations agree with each other very well [155]. Taking into account the considered orientation of axial-symmetric nuclei in searching for the value of the lowest barrier height, we rewrite the expression from Ref. [95] in a simple form,

$$\begin{aligned} V_{\rm C}(r) = &\frac{Z_1 Z_2 e^2}{r}\Bigg\{1 + \sum_{L\geqslant 1}[f_{L1}(r,R_{01})\beta_{L1} + f_{L1}(r,R_{02})\beta_{L2}] \\ &+ f_2(r,R_{01})\beta_{21}^2 + f_2(r,R_{02})\beta_{22}^2 \\ &+ f_3(r,R_{01},R_{02})\beta_{21}\beta_{22}\Bigg\}, \end{aligned} \tag{36}$$

where

$$f_{L1}(r,R_{0i}) = \frac{3R_{0i}^L}{2\sqrt{\pi(2L+1)}r^L}, \tag{37}$$

$$f_2(r,R_{0i}) = \frac{3R_{0i}^2}{7\pi r^2} + \frac{9R_{0i}^4}{14\pi r^4}, \tag{38}$$

$$f_3(r,R_{01},R_{02}) = \frac{27R_{01}^2R_{02}^2}{10\pi r^4}. \tag{39}$$

This expression takes into account the linear and quadratic terms in the quadrupole deformation parameters, and the linear terms of high-multipolarity deformation parameters. The volume correction, which appears in the second order of the quadrupole deformation parameter and is important for heavy systems, is taken into account in this expression.

The nuclei forming the DNS after penetration of the fusion barrier are excited. Therefore, the moment of inertia of the DNS can be approximated well in the framework of the solid-state model. The centrifugal potential energy of DNS nuclei is

$$V_\ell(r,\{\beta_{L1}\},\{\beta_{L2}\}) = \frac{\hbar^2\ell(\ell+1)}{2(\mu r^2 + J_1 + J_2)}, \tag{40}$$

where

$$J_i = (2/5)m_n R_{0i}^2 A_i(1 + \sqrt{5/(16\pi)}\beta_{2i}) \tag{41}$$

is the moment of inertia of nucleus i, and m_n is the nucleon mass. Here we take into account only quadrupole deformation, because the contribution of higher multipolarities to the moment of inertia is negligible.

The incident nuclei participating in cold-fusion reactions have spherical equilibrium shapes. The nuclei involved in the DNS evolution are deforming due to the interaction between them. The deformation energy of the nucleus induced by a deviation from the spherical shape consists of the surface and Coulomb contributions. In the liquid-drop approximation [156], this energy is given as

$$E_{{\rm def}i}^{\rm ld}(\{\beta_{Li}\}) = \sum_{L=2}^{4} C_{LA_iZ_i}^{\rm ld}\frac{\beta_{Li}^2}{2}, \tag{42}$$

where

$$C_{LA_iZ_i}^{\rm ld} = \frac{(L-1)(L+2)b_{\rm surf}A_i^{2/3}}{4\pi} - \frac{3(L-1)e^2Z_i^2}{2\pi(2L+1)R_{0i}} \tag{43}$$

is the surface stiffness coefficient obtained in the liquid-drop approximation, and $b_{\rm surf}$ is the surface coefficient of the mass formula [94].

We can also evaluate the realistic deformation energy of a nucleus at small surface deformations in the framework of the shell correction method [104-107], and approximate the dependence of this energy on the deformation parameters by

$$E_{{\rm def}i}^{\rm sc}(\{\beta_{Li}\}) = \sum_{L=2}^{4} C_{LA_iZ_i}^{\rm sc}\frac{\beta_{Li}^2}{2}. \tag{44}$$

Here $C_{LA_iZ_i}^{\rm sc}$ is the total surface stiffness coefficient obtained with the shell correction method. Using the shell-correction method, we can split both the deformation energy and the stiffness coefficient into shell-correction and liquid-drop parts:

$$\begin{aligned} E_{{\rm def}i}^{\rm sc}(\{\beta_{Li}\}) =& E_{{\rm def}i}^{\rm shell}(\{\beta_{Li}\}) + E_{{\rm def}i}^{\rm ld}(\{\beta_{Li}\}) \\ =& \sum_{L=2}^{4}[C_{LA_iZ_i}^{\rm shell} + C_{LA_iZ_i}^{\rm ld}]\frac{\beta_{Li}^2}{2} \\ =& \sum_{L=2}^{4}\left[\left(\frac{C_{LA_iZ_i}^{\rm sc}}{C_{LA_iZ_i}^{\rm ld}} - 1\right) + 1\right]C_{LA_iZ_i}^{\rm ld}\frac{\beta_{Li}^2}{2}. \end{aligned} \tag{45}$$

The deformation energy of a nucleus at small surface

deformations can also be obtained in the harmonic oscillator model [156, 157]. In this model the deformation energy of a nucleus is described as

$$E^{\rm ho}_{{\rm def}i}(\{\beta_{Li}\}) = \sum_{L=2}^{4} C^{\rm ho}_{LA_iZ_i}\frac{\beta^2_{Li}}{2}. \quad (46)$$

Here $C^{\rm ho}_{LA_iZ_i}$ is the surface stiffness coefficient in the harmonic oscillator model, which is connected to the energy $\mathcal{E}_{LA_iZ_i}$ and the total zero-point amplitude $\beta^0_{LA_iZ_i}$ of the surface oscillations (or the transition probability for exciting the surface oscillations $B(E,0\to L)$) [156, 157],

$$C^{\rm ho}_{LA_iZ_i} = \frac{(2L+1)\mathcal{E}_{LA_iZ_i}}{2(\beta^0_{LA_iZ_i})^2} = \left(\frac{3ZeR^L}{4\pi}\right)^2\frac{(2L+1)\mathcal{E}_{LA_iZ_i}}{2B(E,0\to L)}. \quad (47)$$

The known experimental values of $\mathcal{E}_{LA_iZ_i}$, $\beta^0_{LA_iZ_i}$, and/ or $B(E,0\to L)$ for nuclei are tabulated for $L=2$ and 3 in Refs. [158, 159]. Note that the coupling of the incident channel with low-energy surface vibration channels is often taken into account in the framework of the harmonic oscillator approach in describing various heavy-ion reactions [101, 102, 113, 115]. The characteristics of heavy-ion reactions depend strongly on the properties of the surface vibrations.

The harmonic oscillator $C^{\rm ho}_{LA_iZ_i}$ and shell-correction $C^{\rm sc}_{LA_iZ_i}$ values of the surface stiffness parameters should be close to each other. Therefore, we rewrite Eq. (45) in the form

$$E^{\rm sc}_{{\rm def}i}(\{\beta_{Li}\}) = \sum_{L=2}^{4}\left[\left(\frac{C^{\rm ho}_{LA_iZ_i}}{C^{\rm ld}_{LA_iZ_i}}-1\right)+1\right]C^{\rm ld}_{LA_iZ_i}\frac{\beta^2_{Li}}{2}. \quad (48)$$

This expression for deformation energy is useful for further application, because using experimental values of $\mathcal{E}_{LA_iZ_i}$, $\beta^0_{LA_iZ_i}$ we find the values of the ratio $C^{\rm ho}_{LA_iZ_i}/C^{\rm ld}_{LA_iZ_i}$, as presented in Table 2. We put $C^{\rm ho}_{LA_iZ_i}/C^{\rm ld}_{LA_iZ_i}=1$ if the experimental data for the evaluation of $C^{\rm ho}_{LA_iZ_i}$ are unknown.

The values of the ratio $C^{\rm ho}_{LA_iZ_i}/C^{\rm ld}_{LA_iZ_i}$ for $L=2,3$ presented in Table 2 have an irregular behaviour from one nucleus to another; see also Refs. [156, 157]. This ratio very strongly deviates from 1 near magic nuclei. The nucleus ^{208}Pb is very stiff for surface quadrupole and octupole distortions, because $C^{\rm ho}_{LA_iZ_i}/C^{\rm ld}_{LA_iZ_i}\gg 1$ for $L=2,3$. In contrast to this, nuclei ^{58}Fe and ^{78}Ge are soft for surface quadrupole distortions, because $C^{\rm ho}_{LA_iZ_i}/C^{\rm ld}_{LA_iZ_i}\ll 1$ for $L=2$. These nuclei are well deformed during the DNS decay.

Typical values of excitation energy of a DNS formed by incident nuclei in cold-fusion reactions with 1–3 evaporated neutrons are in the range 15–40 MeV. The amplitudes of shell correction energy at such excitation energies are approximately reduced 2–4 times [129-131, 160-166]. We expect a similar effect for the value of the stiffness parameter, which should approach the hydrodynamical one at high excitation energies.

Table 2. The ratio $C^{\rm ho}_{LA_iZ_i}/C^{\rm ld}_{LA_iZ_i}$ obtained using the experimental properties of the low-energy surface vibrational states with multiplicities $L=2$ [158] and $L=3$ [159]. We put $C^{\rm ho}_{LA_iZ_i}/C^{\rm ld}_{LA_iZ_i}=1$ in the case of unknown experimental properties of the low-energy surface vibrational states for a given multiplicity and nucleus.

Nucleus	$C^{\rm ho}_{LA_iZ_i}/C^{\rm ld}_{LA_iZ_i}$		
	$L=2$	$L=3$	$L=4$
^{50}Ti	2.03	1.46	1
^{52}Cr	12	3.15	1
^{54}Cr	0.45	1	1
^{58}Fe	0.36	2.0	1
^{64}Ni	1.46	1.36	1
^{70}Zn	0.54	0.56	1
^{78}Ge	0.33	1	1
^{208}Pb	44.9	2.2	1

Moreover, the single-particle spectra of nuclei near the contact point became more homogeneous due to level splitting and shifting induced by the nucleus-nucleus interaction. This leads to a reduction of the amplitudes of the shell correction energies in interacting nuclei, see also Eq. (8). Consequently, the values of realistic surface stiffness coefficient of nuclei should approach the liquid-drop one at small distances between them due to the nucleus-nucleus interaction.

Taking into account the excitation energy and nucleus-nucleus interaction effects on the shell correction energies, we modify Eq. (48) as

$$E_{{\rm def}i}(\{\beta_{Li}\}) = \sum_{L=2}^{4}\left[\left(\frac{C^{\rm ho}_{LA_iZ_i}}{C^{\rm ld}_{LA_iZ_i}}-1\right)k_{LA_iZ_i}+1\right]\times\frac{C^{\rm ld}_{LA_iZ_i}\beta^2_{Li}}{2}. \quad (49)$$

Here $k_{LA_iZ_i}\approx 0.1$ is the parameter which describes the attenuation of the shell-correction effect on the surface stiffness coefficient of the incident nuclei forming the DNS in the cold-fusion reactions. If $C^{\rm ho}_{LA_iZ_i}=C^{\rm ld}_{LA_iZ_i}$ then the deformation energy is determined by the liquid-drop properties and is independent of $k_{LA_iZ_i}$. Note that the deformation energy is only defined by the liquid drop properties in the framework of various versions of the DNS model of SHN production [60-75, 78].

The double-magic target nucleus ^{208}Pb and magic or close to magic projectile nuclei are involved in the incid-

ent channel of the cold-fusion reactions. Therefore, we should take into account a realistic surface stiffness of nuclei in calculating the width $\Gamma^{\rm DNS}_{\rm def}(E,\ell)$. The width $\Gamma^{\rm DNS}_{\rm def}(E,\ell)$ is linked to $B^{\rm DNS}_{\ell,\rm def}$, which is calculated with the help of Eqs. (31)-(41), (43), (47), (49). The value of $B^{\rm DNS}_{\ell,\rm def}$ rises with a rising $C^{\rm ho}_{2A_i82}/C^{\rm ld}_{2A_i82}$, because the barrier takes place at smaller values of the deformation parameter of nuclei. Using very stiff nuclei in the cold fusion reaction leads to a higher value of $B^{\rm DNS}_{\ell,\rm def}$ and, as a result, a smaller value of $\Gamma^{\rm DNS}_{\rm def}(E,\ell)$. This leads to an increasing probability of compound nucleus formation $P(E,\ell)$ described by Eq. (12). Conversely, fusion reactions between soft nuclei have a smaller value of $B^{\rm DNS}_{\ell,\rm def}$ and, as a result, a higher value of $\Gamma^{\rm DNS}_{\rm def}(E,\ell)$ and smaller value of $P(E,\ell)$.

The correlation between the surface stiffness of incident nuclei and the production cross sections is clearly observed experimentally. For example, the values of $C^{\rm ho}_{2A_i82}/C^{\rm ld}_{2A_i82}$ for nuclei ^{208,206,204}Pb obtained using data from Ref. [158] are, respectively, close to 45, 25, 17. The values of cross-section maxima for reactions ^{208,206,204}Pb(^{48}Ca,$2n$)^{254,252,250}No are $3\cdot10^6, 4\cdot10^5, 7\cdot10^3$ b [5, 6], correspondingly. So, we clearly see that reactions with stiffer target nuclei have higher values of the SHN production cross section. (Note that other effects may also contribute to the cross-section values.) The surface stiffness effect may be also significant for the synthesis of SHN with $Z>118$ in hot fusion reactions, when the stiff projectile ^{48}Ca is substituted by a softer one such as ^{50}Ti or similar.

Let us consider the other barriers related to the corresponding decay widths used in our model. The barrier $B^{\rm DNS}_{\ell,\rm DIC} = B^{\rm DNS}_{0,\ell,\rm DIC} + Q_{\rm tr}$ is defined as the barrier between deformed contacting nuclei formed after nucleon transfer from the heavy nucleus to the light one, where $Q_{\rm tr}$ is the transfer reaction Q-value evaluated with the help of an atomic mass table [108]. This barrier takes place in evolution of the initial DNS system to a more symmetric one. The DNS after passing the barrier $B^{\rm DNS}_{\ell,\rm DIC}$ can decay into two scattered nuclei with new nucleon composition, or the nucleon exchange between nuclei can continue further. The interaction potential energy of touching nuclei after nucleon exchange $B^{\rm DNS}_{0,\ell,\rm DIC}$ is calculated in a similar way as $B^{\rm DNS}_{\ell,\rm def}$. The barrier $B^{\rm DNS}_{\ell,\rm DIC}$ is the minimal value of the barriers related to various nucleon transfer paths from the incident DNS to the more symmetric one. Substituting the obtained value of the barrier into Eq. (29), we can find the width $\Gamma^{\rm DNS}_{\rm DIC}(E,\ell)$.

Compound nucleus formation using the DNS path is related to the barrier $B^{\rm DNS,tr}_{\ell,\rm CN}$, which takes place in nucleon transfer from the light nucleus to the heavy one. The values of $B^{\rm DNS,tr}_{\ell,\rm CN}$ for every system formed along various multi-nucleon transfer paths is evaluated similarly to $B^{\rm DNS}_{\ell,\rm DIC}$. The surface deformations of both nuclei are also taken into account. The barrier $B^{\rm DNS,tr}_{\ell,\rm CN}$ is the minimal value among the barriers related to various paths from the DNS formed by incident nuclei to the compound nucleus. The width $\Gamma^{\rm DNS,tr}_{\rm CN}(E,\ell)$ is calculated substituting the value of $B^{\rm DNS,tr}_{\ell,\rm CN}$ into Eq. (29).

The width $\Gamma^{\rm DNS,f}_{\rm CN}(E,\ell)$ is related to the barrier

$$B^{\rm DNS,f}_{\ell,\rm CN} = B^{\rm DNS,f}_{0,\rm CN} + \frac{\hbar^2\ell(\ell+1)}{2J^{\rm fus}_{\rm CN}} + Q_{\rm CN}. \tag{50}$$

Here $B^{\rm DNS,f}_{0,\rm CN}$ is the height of a corresponding saddle point evaluated relative to the ground state of the compound nucleus using the potential energy surface presented in Figs. 1-2, $J^{\rm fus}_{\rm CN}$ is the moment of inertia of the compound nucleus at the saddle point, and $Q_{\rm CN}$ is the Q-value of the compound nucleus formation evaluated with the help of an atomic mass table [108]. The width $\Gamma^{\rm DNS,f}_{\rm CN}(E,\ell)$ is obtained using Eq. (23) and the value $B^{\rm DNS,f}_{\ell,\rm CN}$.

The widths related to the intermediate state can be found in a similar way to the width $\Gamma^{\rm DNS,f}_{\rm CN}(E,\ell)$.

After obtaining the values of all widths we can determine the probability of compound nucleus formation. Now we can determine the survival probability of the compound nucleus.

C. Survival probability of the compound nucleus

The survival probability of the compound nucleus formed in the cold-fusion reaction is related to the competition between the evaporation of x neutrons and fission. It can be approximated by the expression

$$\begin{aligned} W^{xn}(E,\ell) =& P_{xn}(E^*_{\rm CN\ell})\frac{\Gamma_{1n}(E^*_1,\ell)}{\Gamma_{1n}(E^*_{1n},\ell)+\Gamma_{\rm f}(E^*_1,\ell)} \\ &\times\frac{\Gamma^{A-1}_{2n}(E^*_2,\ell)}{\Gamma^{A-1}_{2n}(E^*_2,\ell)+\Gamma^{A-1}_{\rm f}(E^*_2,\ell)}\times\ldots \\ &\times\frac{\Gamma^{A-x+1}_{xn}(E^*_x,\ell)}{\Gamma^{A-x+1}_{xn}(E^*_x,\ell)+\Gamma^{A-x+1}_{\rm f}(E^*_x,\ell)}. \end{aligned} \tag{51}$$

Here $P_{xn}(E^*)$ is the realization probability of the xn-evaporation channel [167], $E^*_{\rm CN\ell} = E - Q_{\rm CN} - \hbar^2\ell(\ell+1)/(2J_{\rm gs})$, and $J_{\rm gs}$ is the ground-state moment of inertia. $E^*_1 = E - Q_{\rm CN}$ is the excitation energy of the compound nucleus formed in the heavy-ion fusion reaction. $\Gamma^{A-y+1}_{yn}(E^*_y,\ell)$ and $\Gamma^{A-y+1}_{\rm f}(E^*_y,\ell)$ are, respectively, the width of neutron emission and the fission width of the compound nucleus formed after emission of $(y-1)$ neutrons. $E^*_y = E^*_{y-1} - B_{n,y-1} - 2T_{y-1}$ is the excitation energy before evaporation of the y-th neutron, where $B_{n,y-1}$ is the separation energy of the $(y-1)$-th neutron. T_{y-1} is the temperature of the compound nucleus after evaporation of $(y-1)$ neutrons and is obtained from $E^*_{y-1} = a_{\rm dens}T^2_{y-1}$, where $a_{\rm dens}$ is

defined by Eqs. (27)-(28).

The width of neutron emission from a nucleus with A nucleons is given as [168]

$$\Gamma_n(E^*,\ell)=\frac{g_n m_n R_n^2}{\pi\hbar^2\rho_{A,\ell}(E^*)}\int_0^{E^*-B_n}\mathrm{d}\varepsilon\,\varepsilon \times\rho_{A-1,\ell}(E^*-B_n-\varepsilon,\ell), \tag{52}$$

where B_n is the neutron separation energy from the nucleus, $\rho_{A,\ell}(E^*)$ and $\rho_{A-1,\ell}(E^*)$ are, correspondingly, the energy level densities of the compound nuclei before and after neutron emission, g_n is the neutron intrinsic spin degeneracy, and R_n is the radius of the neutron-nucleus interaction.

The fission width of the nucleus depends on the fission barrier height, which consists of the liquid-drop and shell-correction contributions in the Strutinsky shell correction prescription [104-107]. The excitation energy of a compound nucleus formed in cold-fusion reactions E^* is in the range 10 to 25 MeV, therefore $T\lesssim 1$ MeV. The liquid-drop part of the fission barrier weakly depends on temperature at $T\lesssim 2$ MeV [160, 169-171]. As a result, the temperature dependence of the shell correction contribution [27, 41, 160-165] induces the temperature dependence of the fission barrier of SHN.

The exponential reduction of the fission barrier of SHN with thermal excitation energy is obtained in the framework of the finite-temperature self-consistent Hartree-Fock+BCS model with Skyrme force in Refs. [129-131, 166]. The exponential dependence of the fission barrier height is also used in Refs. [41, 60, 61, 63-65, 67-75, 78, 81, 114, 160]. We also consider the exponential decrease of the fission barrier with the excitation energy, and define the fission barrier of excited rotating nuclei as

$$B_{\rm f}(\varepsilon,\ell)=B_{\rm f}^{\rm ld}+B_{\rm f}^{\rm sh}e^{-\gamma_D\varepsilon}+\frac{\hbar^2\ell(\ell+1)}{2}\left[\frac{1}{J_{\rm s}}-\frac{1}{J_{\rm gs}}\right]. \tag{53}$$

Here $B_{\rm f}^{\rm ld}$ and $B_{\rm f}^{\rm sh}(\varepsilon)$ are the liquid-drop and shell-correction contributions to the fission barrier, and γ_D is the damping parameter [27, 41, 114, 129-131, 160]. The last line of the equation describes the rotational contribution to the barrier. $J_{\rm gs(s)}=m_n(2/5)R_0^2A(1+\sqrt{5/(16\pi)}\beta_{\rm gs(s)})$ and $\beta_{\rm gs(s)}$ are, respectively, the ground-state (fission saddle-point) moment of inertia and the quadrupole deformations of the compound nucleus.

The dependence of the fission barrier of SHN on the excitation energy should be taken into account in the evaluation of the survival probability. The Bohr-Wheeler expression for the fission width [116, 168] is obtained in the transition state approach with the fission barrier independent of the excitation energy. This expression is not consistent with the barrier dependence on the excitation energy [172, 173].

The number of states over the barrier increases with the thermal reduction in fission barrier height. Taking into account both the dependence of the fission barrier on the excitation energy and the rising of the number of states over the energy-dependent fission barrier, we derive a new expression for the fission width in the form [160]

$$\Gamma_{\rm f}(E^*,\ell)=\frac{2}{2\pi\rho_{A,\ell}(E^*)}\int_0^{\varepsilon_{\max}}\mathrm{d}\varepsilon\frac{\rho_{A,\ell}(\varepsilon)}{N_{\rm tot}}N_{\rm saddle}(\varepsilon). \tag{54}$$

Here the ratio $\rho(\varepsilon)/N_{\rm tot}$ is the probability of finding the fissioning nucleus with intrinsic thermal excitation energy ε in the fission transition state, $N_{\rm tot}=\int_0^{\varepsilon_{\max}}d\varepsilon\rho_{A,\ell}(\varepsilon)$ is the total number of states available for fission in the case of the energy-dependent fission barrier, $N_{\rm saddle}(\varepsilon)=\int_{\varepsilon}^{E-B_{\rm f}(\varepsilon)}\mathrm{d}e\rho_{A,\ell}(e)$ is the number of states available for fission at ε and barrier value $B_{\rm f}(\varepsilon)$. $\varepsilon_{\max}$ is the maximum value of the intrinsic thermal excitation energy of the nucleus at the saddle point, which is determined as the solution of the equation

$$\varepsilon_{\max}+B_{\rm f}(\varepsilon_{\max},\ell)=E^*. \tag{55}$$

This equation is related to the energy conservation law, i.e. the sum of thermal $\varepsilon_{\max}$ and potential $B_{\rm f}(\varepsilon_{\max},\ell)$ energies at the saddle point equals the total excitation energy E^*.

The difference between the Bohr-Wheeler fission width [116] and $\Gamma_{\rm fiss}(E^*,\ell)$ is discussed in Refs. [114, 160]. Note that $\Gamma_{\rm f}(E^*,\ell)$ is equal to the Bohr-Wheeler fission width in the case of the energy-independent fission barrier [160].

III. DISCUSSION

In this section we compare the theoretical values of the SHN production cross sections obtained in the framework of our model for various cold fusion reactions with experimental measurements. At the beginning we would like to point out some important experimental features of the cross-section data of SHN production.

The experimental cross sections for the reaction ^{208}Pb(^{64}Ni,n)^{271}Ds have been measured at Gesellschaft fur Schwerionenforschung (GSI) [2, 12], Lawrence Berkeley National Laboratory (LBNL) [15, 19], and the Institute of Physical and Chemical Research (RIKEN) [14]. Unfortunately, the collision energies and values of the cross section at the maxima obtained for this reaction

at the different laboratories are different. The difference between the lowest [2, 12] and highest [14] collision energies of the maxima of the cross sections for the reaction ^{208}Pb(^{64}Ni,n)^{271}Ds obtained by the different experiments is close to 5 MeV (see also Fig. 7 and Ref. [19]). This energy difference is very large, because the cold fusion reaction usually takes place at sub-barrier collision energies. The values of the sub-barrier fusion cross section may change by several orders of magnitude with a variation of the collision energy of 5 MeV. Such changes of the sub-barrier fusion cross section with collision energy are typical for light and medium heavy-ion systems; see, for example, Refs. [27, 96, 101, 102, 113, 115]. There should be a similar dependence on the capture process in the case of cold fusion reactions.

The targets used in experiments for SHN synthesis are thick. The SHN production reaction may take place when the projectile is just entering into the target or just before the projectile escapes the target. The beam loss energy in the target is close to 3–4 MeV [19]. As a rule, the collision energies in the middle of the target or the laboratory beam energies are pointed in experimental works. In these cases, the reaction may take place at energies approximately ±2 MeV or 4 MeV lower than the experimentally pointed ones.

The maximal values of the cold-fusion cross section measured in different laboratories are strongly varied too. For example, the maximal values of the cross section for the reaction ^{208}Pb(^{50}Ti,n)^{257}Rf presented in Refs. [7-9] differ by about a factor of three (see also Fig. 3). Note that the number of reaction events is relatively high for this reaction. Due to this the statistical errors are low in both experiments. In contrast to this, only 1 or 2 reaction events are obtained in experiments for the production of very heavy SHN in cold-fusion reactions. Therefore, the experimental errors of the cross section are very high (see, for example, Fig. 8).

Due to these reasons, the exact values of the heavy-ion collision energies at which the SHN form in experiments and the cross-section values are not yet well-defined. Consequently, there is no way to describe the cross-section of SHN production precisely. Therefore, we use a "soft" criterion of the agreement between the experimental data and the theoretical calculations. This criterion assumes that we describe both the maximal value of the cross section for some experimental measurement with 50% accuracy and the energy position of the maximum of the cross section with a precision of several MeV. Moreover, we see the more physical sense in the smaller changes of the fitting parameters for the nearest reactions, than in better agreement with the data. Below we will point out when the fitting parameters are drastically changed for the nearest reactions and discuss the reason for these changes.

A. Reaction ^{208}Pb(^{50}Ti,xn)$^{258-x}$Rf

The values of the cross sections for the reactions ^{208}Pb(^{50}Ti,xn)$^{258-x}$Rf with $x = 1$ and 2 have been measured at GSI [7, 8] and LBNL [9]. The experimental cross sections for the reaction ^{208}Pb(^{50}Ti,3n)^{255}Rf have only been obtained at GSI [7, 8]. We calculate the cross sections for these reactions in the framework of our model and compare the obtained values with the experimental data in Fig. 3. Our results agree well with the LBNL data [9], but the GSI data shift to lower collision energies relative to both the LBNL data and our results, see Fig. 3. Taking into account the "soft" criterium we conclude that the experimental cross sections for the reactions ^{208}Pb(^{50}Ti,xn)$^{258-x}$Rf with $x = 1 \div 3$ are described well in the framework of our model.

The parameters of the model used in the calculation of the reactions ^{208}Pb(^{50}Ti,xn)$^{258-x}$Rf are presented in Tables 2-4. Note that these values of parameters are not unique. It is also possible to describe the data by choosing other slightly different values of the parameters.

The starting values of the fission barrier $B_f(0,0)$ and the compound nucleus formation barrier $B_{0,CN}^{DNSf}$ are extracted from Fig. 1. However, the final values of the parameters presented in Tables 3-4 are chosen by fine fitting of the experimental data. The values of these barriers given in the tables are close to those extracted from Fig. 1. The ground state β_{gs} and saddle point β_{sp} deformations of fissioning nuclei are taken from Fig. 1.

The experimental information on the fission barrier height in SHN is very poor. The values of the fission barrier obtained in various models [122, 123, 124, 127-138] for SHN are very different. The difference is more than 100% in some cases [138]. The reasons for the uncertain-

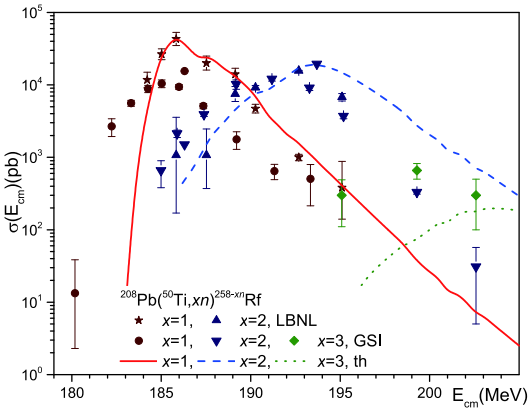

Fig. 3. (color online) Comparison of our theoretical calculations of the cross sections for reactions ^{208}Pb(^{50}Ti,xn)$^{258-x}$Rf with $x = 1,2$ and 3 with available experimental data. The cross sections for reactions ^{208}Pb(^{50}Ti,xn)$^{258-x}$Rf with $x = 1$ and 2 are measured in Refs. [7, 8] (GSI) and [9] (LBNL) and the cross sections for reaction ^{208}Pb(^{50}Ti,3n)^{255}Rf are from Ref. [7, 8] (GSI).

Table 3. The liquid-drop $B_{\rm f}^{\rm ld}$ and shell $B_{\rm f}^{\rm sh}$ contributions to the fission barriers $B_{\rm f}^{0}=B_{\rm f}^{\rm ld}+B_{\rm f}^{\rm sh}$ of nuclei, the ground state $\beta_{\rm gs}$ and saddle point $\beta_{\rm sp}$ deformations of fissioning nuclei, and the damping parameter of the fission barrier γ_D. The fission barrier values $B_{\rm f}$ obtained in Refs. [127, 135] are also presented. The values of barriers are given relative to the ground-state energy of the compound nucleus in MeV. The values of γ_D are presented in MeV^{-1}.

Nucleus	$B_{\rm f}^{\rm ld}$	$B_{\rm f}^{\rm sh}$	$B_{\rm f}^{0}$	$B_{\rm f}^{[127]}$	$B_{\rm f}^{[135]}$	$\beta_{\rm gs}$	$\beta_{\rm sp}$	γ_D
^{258}Rf	0.5	6.3	6.8	5.0	5.65	0.2	0.4	0.105
^{257}Rf	0.5	6.1	6.6	5.6	6.02	0.2	0.4	0.105
^{256}Rf	0.5	6.5	7.0	5.3	6.26	0.2	0.4	0.105
^{262}Sg	0.4	3.7	4.1	4.3	5.91	0.2	0.4	0.07
^{261}Sg	0.4	3.3	3.7	4.7	5.88	0.2	0.4	0.07
^{260}Sg	0.4	4.8	5.2	4.6	5.84	0.2	0.4	0.11
^{259}Sg	0.3	3.0	3.3	4.9	5.82	0.2	0.4	0.11
^{266}Hs	0.5	5.7	6.3	3.5	6.26	0.2	0.4	0.10
^{265}Hs	0.5	4.2	4.7	3.5	6.26	0.2	0.4	0.10
^{272}Ds	0.4	3.7	4.1	2.2	7.31	0.2	0.4	0.04
^{271}Ds	0.3	3.5	3.8	2.2	6.92	0.2	0.4	0.04
^{278}Cn	0.2	2.3	2.5	1.9	5.99	0.0	0.3	0.04
^{277}Cn	0.3	2.6	2.9	2.0	6.36	0.0	0.3	0.04
^{286}Fl	0.4	4.2	4.6	4.1	9.00	0.0	0.3	0.05
^{285}Fl	0.4	4.0	4.4	2.7	8.82	0.0	0.3	0.05

Table 4. Barrier values of the fusion trajectory at the formation of the compound nucleus from the DNS $B_{\rm 0,CN}^{\rm DNS,f}$ and the parameter Δ_B. The values of Δ_B and $B_{\rm 0,CN}^{\rm DNS,f}$ are given in MeV. The barrier values $B_{\rm 0,CN}^{\rm DNS,f}$ are given relative to the ground state energy of the compound nucleus. The last column shows the laboratory in which the experimental data were obtained for the reaction.

Reaction	Δ_B	$B_{\rm 0,CN}^{\rm DNS,f}$	Exp. lab.
^{208}Pb+^{50}Ti	5.0	12.5	GSI, LBNL
^{208}Pb+^{52}Cr	4.0	14.7	LBNL
^{208}Pb+^{54}Cr	11.0	11.1	GSI
^{208}Pb+^{58}Fe	7.0	10.6	GSI, RIKEN
^{208}Pb+^{64}Ni	6.5	6.2	GSI,LBNL,RIKEN
^{208}Pb+^{70}Zn	4.0	2.7	GSI, RIKEN
^{208}Pb+^{78}Ge	4.0	4.9	

ties in the predictions of fission barrier heights in SHN have been discussed in Ref. [138]. Therefore, it is difficult to prefer any model for the barrier calculation. Nevertheless, we present the fission barrier values $B_{\rm f}$ obtained in Refs. [127, 135] in Table 3 for a comparison. The values of barriers $B_{\rm f}(0,0)=B_{\rm f}^{\rm ld}+B_{\rm f}^{\rm sh}$ obtained with the help of Fig. 1 and after fine fitting of the data are within the range of barrier values found in other approaches. The values of the liquid-drop $B_{\rm f}^{\rm ld}$ and shell $B_{\rm f}^{\rm sh}$ contributions to the fission barriers of nuclei and the ground state $\beta_{\rm gs}$ and saddle point $\beta_{\rm sp}$ deformations of fissioning nuclei are near the corresponding values from Refs. [124]. The values of the liquid-drop $B_{\rm f}^{\rm ld}$ contribution to the fission barrier are close to 10% of the shell contribution $B_{\rm f}^{\rm sh}$.

The values of the damping parameter of the fission barrier γ_D depend on the numbers of protons and neutrons in the nucleus and are in the range from ≈ 0.1 to 0.03 MeV^{-1} [129-131]. The values of γ_D presented in Table 3 are in this range. The influence of this parameter on the evaporation characteristics have been widely discussed. For details, see Refs. [27, 41, 51, 60, 61, 65, 67-70, 72-75, 81, 114, 129-131, 160]. Note that parameters γ_D and γ in Eq. (27) are different, because they are obtained by the fitting of different physical quantities.

As has been pointed out earlier, accurate values of the collision energies of reactions leading to SHN are not known due to the thick target and the differences in the experimental data obtained by various laboratories. Therefore, it is reasonable to fit the maximum of the theoretical cross section using the parameter Δ_B, because the position of the maximum depends strongly on it. The parameter Δ_B is linked to the width of the fusion barrier distribution g, see Eqs. (4)-(5) and related text. The value of g is not known experimentally. The value of Δ_B obtained from the fit of the data [9] is given in Table 4. The value of Δ_B presented in Table 4 corresponds to the width of the barrier distribution $g=3.3$ MeV, which is in the range of typical values of $g=2-4$ MeV used in other models [51, 66, 72-74]. Note that the GSI data can be fitted by using larger values of Δ_B.

The position of the barrier $B_{\rm 0,CN}^{\rm DNS,f}$ corresponds to the contacting near-spherical incident nuclei forming the DNS, see Fig. 1. Due to this the moment of inertia related to this barrier, see Eq. (50), is calculated as $J_{\rm CN}^{\rm fus}\approx\mu(R_1+R_2)^2$.

B. Reaction ^{208}Pb(^{52}Cr,xn)$^{260-x}$Sg

The values of the cross sections for the reactions ^{208}Pb(^{52}Cr,xn)$^{260-x}$Sg with $x=1$ and 2 have been measured at LBNL [11]. The results calculated in the framework of our model agree well with the experimental data, see Fig. 4. The parameters of the model used in the calculation of these reactions are presented in Tables 2-4. The values of the parameters are chosen in a similar way to those for the reactions ^{208}Pb(^{50}Ti,xn)$^{258-x}$Rf. The parameter values for the reactions ^{208}Pb(^{52}Cr,xn)$^{260-x}$Sg are close to the corresponding ones for ^{208}Pb(^{50}Ti,xn)$^{258-x}$Rf. However, we use a smaller value of the dissipation parameter γ_D, see Table 3, which is responsible for attenu-

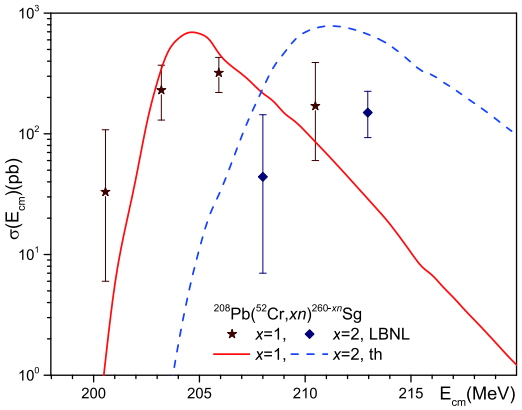

Fig. 4. (color online) Comparison of our theoretical calculations of the cross sections for reactions ^{208}Pb(^{52}Cr,xn)$^{260-x}$Rf with $x=1$ and 2 with the experimental data measured in Ref. [11] (LBNL).

ation of the shell contribution of the fission barrier. Recall that the value of γ_D depends strongly on the numbers of protons and neutrons in the nucleus [129-131].

C. Reaction ^{208}Pb(^{54}Cr,xn)$^{262-x}$Sg

The cross sections for the reactions ^{208}Pb(^{54}Cr,xn)$^{262-x}$Sg with $x=1$ and 2 have been measured at GSI [10]. We calculate the cross sections for these reactions in the framework of our model. Our model describes the experimental data well, as seen in Fig. 5.

The parameters of the model used in calculation of the reactions ^{208}Pb(^{54}Cr,xn)$^{262-x}$Sg are given in Tables 2-4. The parameters presented in Table 4 are similar to the corresponding ones for ^{208}Pb(^{50}Ti,xn)$^{258-x}$Rf and ^{208}Pb(^{52}Cr,xn)$^{260-x}$Sg.

The maxima of the SHN cross sections for reactions measured at GSI took place at smaller collision energies than those measured at other laboratories. Therefore, for the sake of the data description, we use the largest value of parameter Δ_B for this reaction in comparison to other reactions, see Table 4. The value of the barrier $B_{0,\mathrm{CN}}^{\mathrm{DNS,f}}$ for ^{208}Pb(^{52}Cr,xn)$^{260-x}$Sg reaction is higher than that for the reaction ^{208}Pb(^{54}Cr,xn)$^{262-x}$Sg, see Table 4. The excitation energy of the compound nucleus at the maximum of the SHN cross section reduces when the maximum is shifted to smaller collision energies. Therefore, we change the parameters related to the survival probability of the compound nucleus. The values of the fission barriers for the nuclei presented in Table 3 are close to those obtained in Refs. [127, 135].

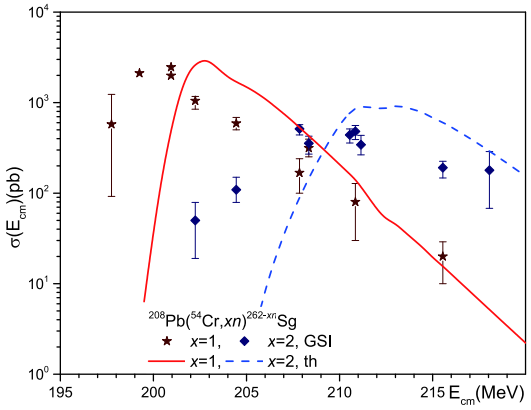

Fig. 5. (color online) Comparison of our theoretical calculations of the cross sections for reactions ^{208}Pb(^{54}Cr,xn)$^{262-x}$Rf with $x=1$ and 2 with the experimental data measured in Ref. [10] (GSI).

D. Reaction ^{208}Pb(^{58}Fe,xn)$^{266-x}$Hs

The values of the cross sections for the reaction ^{208}Pb(^{58}Fe,1n)^{265}Hs have been measured at GSI [2, 12], and those for the reactions ^{208}Pb(^{58}Fe,xn)$^{266-x}$Hs with $x=1$ and 2 have been obtained at RIKEN [13]. The cross sections for these reactions calculated in the framework of our model agree well with the experimental data, as shown in Fig. 6.

The difference in the collision energy values of the cross section maxima measured at GSI and RIKEN for the reaction ^{208}Pb(^{58}Fe,1n)^{265}Hs is close to 4 MeV, see Fig. 6. It is reasonable to set the maximum of the cross section in our model for the reaction ^{208}Pb(^{58}Fe,1n)^{265}Hs at a collision energy between those obtained at GSI and RIKEN. Due to this, the value of Δ_B for this reaction lies between those for reactions with ^{52}Cr and ^{54}Cr projectiles, see Table 4. The width of the cross section peaks are close to the experimental ones.

The other parameters of the model used in the calculation of the reactions ^{208}Pb(^{58}Fe,xn)$^{266-x}$Hs are presented in Tables 2-4. The values of the parameters are

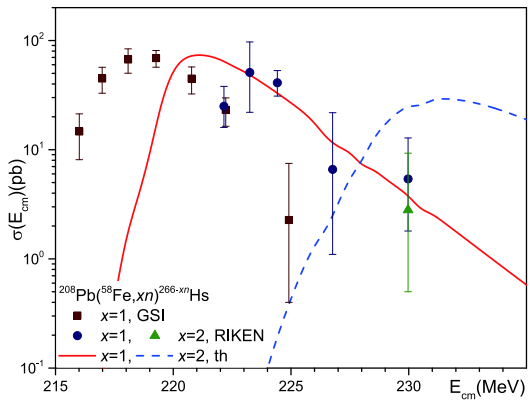

Fig. 6. (color online) Comparison of our theoretical calculations of the cross sections for reactions ^{208}Pb(^{58}Fe,xn)$^{266-x}$Hs with x=1 and 2 with available experimental data. The cross sections for reaction ^{208}Pb(^{58}Fe,1n)^{265}Hs are measured in Refs. [2, 12] (GSI) and those for reactions ^{208}Pb(^{58}Fe,xn)$^{266-x}$Hs x=1 and 2 are from Ref. [13] (RIKEN).

chosen in a similar way to other reactions.

Our value for the fission barrier for ^{266}Hs is very close to that obtained in Ref. [135] and larger the one presented in Ref. [127]. Our value for the fission barrier for ^{265}Hs lies between those obtained in Refs. [127, 135].

E. Reaction ^{208}Pb(^{64}Ni,xn)$^{272-x}$Ds

The cross sections for the reaction ^{208}Pb(^{64}Ni,1n)^{271}Ds have been measured at GSI [2, 12], LBNL [15], and RIKEN [14]. We calculate the cross sections for the reactions ^{208}Pb(^{64}Ni,xn)$^{272-x}$Ds with $x = 1$ and 2 in the framework of our model. The calculated values agree well with the available experimental data, as seen in Fig. 7.

The parameters of the model used in the calculation of reactions ^{208}Pb(^{64}Ni,1n)^{271}Ds are given in Tables 2-4. We select the value of parameter Δ_B so that the theoretical peak of the cross sections lies close to the RIKEN data. This value of parameter Δ_B is close to those obtained for a description of the RIKEN data with other projectiles, see Table 4. The value of the barrier of the fusion trajectory from the DNS to the compound nucleus $B_{0CN}^{DNS,f}$ is estimated using Fig. 2. We see that the values $B_{0,CN}^{DNSf}$ decrease with rising projectile mass, see Figs. 1-2 and Table 4. The smallest value of the dissipation parameter γ_D is used for this reaction, see Table 3. The values of other parameters are chosen in a similar way as before.

The cross-section points of this reaction measured at GSI, see Fig. 7, are located at smaller collision energies than those measured at RIKEN and the results obtained in our model. The difference in the position of the cross-section maxima for this reaction measured at different laboratories is close to 5 MeV.

The maximum of the cross section for the reaction with 2n emission ^{208}Pb(^{64}Ni,2n)^{270}Ds is located at high beam energy, which is not used in any experiments. The calculated value of cross section in the maximum for the reaction ^{208}Pb(^{64}Ni,2n)^{270}Ds is much lower than that for ^{208}Pb(^{64}Ni,1n)^{271}Ds, see Fig. 7.

F. Reaction ^{208}Pb(^{70}Zn,xn)$^{278-x}$Cn

The cross sections for the reaction ^{208}Pb(^{70}Zn,1n)^{277}Cn have been measured at GSI [2, 16] and RIKEN [17, 18]. We have calculated the cross sections for this reaction in the framework of our model. Our model describes the data from both laboratories well, by the corresponding parameter choice, as seen in Fig. 8. The values of parameters used in our calculations of the reactions ^{208}Pb(^{70}Zn,xn)$^{277-x}$Cn, with x = 1 and 2, are presented in Tables 2-4.

The value of barrier $B_{0,CN}^{DNS,tr}$ for this system obtained in our approach is 269.3 MeV, see Table 5. This value is close to that evaluated in Ref. [67], 20.98 MeV - Q_{CN} = 20.98 MeV + 244.2 MeV = 265.18 MeV. As pointed out

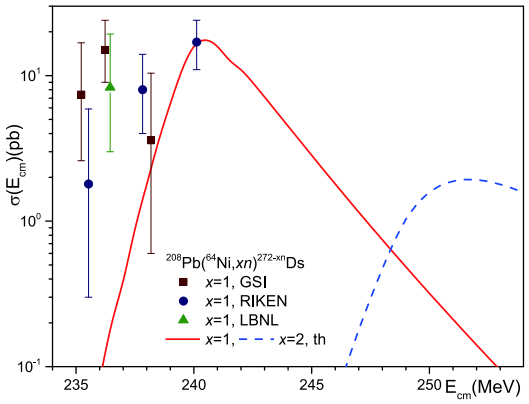

Fig. 7. (color online) Comparison of our theoretical calculations of the cross sections for reactions ^{208}Pb(^{64}Ni,1n)^{271}Ds with available experimental data. The cross sections for this reaction are measured in Refs. [2, 12] (GSI), [14] (RIKEN) and [15] (LBNL). The theoretical calculation of the cross section for reaction ^{208}Pb(^{64}Ni,2n)^{270}Ds is also presented.

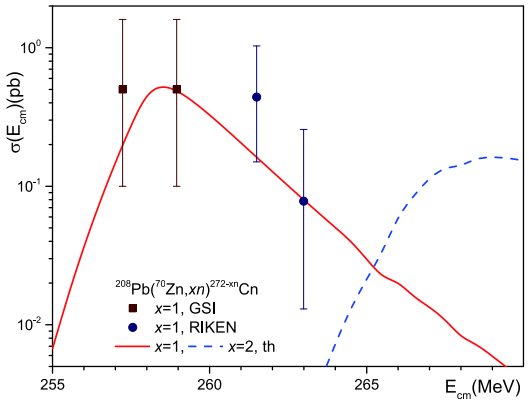

Fig. 8. (color online) Comparison of our theoretical calculation of the cross section for reactions ^{208}Pb(^{70}Zn,1n)^{277}Cn with available experimental data. The cross sections for this reaction are measured in Refs. [2, 16] (GSI) and [17, 18] (RIKEN). The theoretical calculation of the cross section for the reaction ^{208}Pb(^{70}Zn,2n)^{276}Cn is also presented.

in Ref. [62], the calculations of the nucleus-nucleus potentials of spherical nuclei in the framework of the DNS model include the Coulomb barriers, which are at least 5 MeV lower than the phenomenological Bass barriers [109]. The values of barriers of the nucleus-nucleus potential for very asymmetric systems with medium or small values of Z_1Z_2 calculated in our approach are close to the Bass barriers [103]. Therefore, such a difference between values of the barrier $B_{0,CN}^{DNS,tr}$ obtained in different approaches is reasonable.

The mechanism of this reaction takes into account the contribution of the intermediate state. This intermediate state is located in the well between the inner and outer fission barriers, see Fig. 2. The inner fission barrier is lower than the outer fission barrier by approximately 1

MeV, see Fig. 2. The height of the barrier related to the decay back to the DNS is higher than the inner fission barriers, see Fig. 2 and Tables 3 and 4. Therefore, the decay of the intermediate state to the compound nucleus is preferential for this reaction. Due to this we put $P_{is} \approx 0.88(0.85)$ for $1n(2n)$ reactions, for a simplification of the calculation.

G. Reaction ^{208}Pb(^{78}Ge,xn)$^{286-x}$Fl

The values of the cross sections for the reaction ^{208}Pb(^{78}Ge,xn)^{285}Fl, for $x=1$ and 2, have not been measured to date. We have calculated the cross sections for these reactions in the framework of our model and present the results in Fig. 9. The values of SHN production cross section are very small for these reactions.

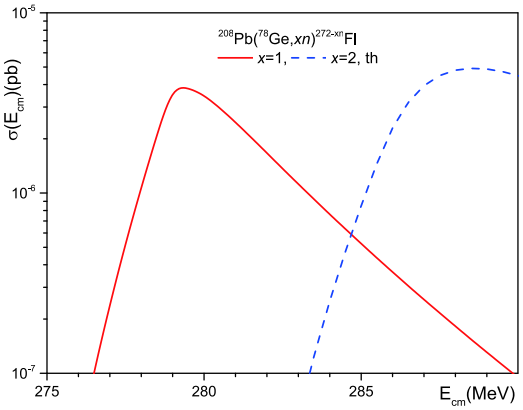

Fig. 9. (color online) Results of calculations of the cross sections for reactions ^{208}Pb(^{78}Ge,xn)$^{286-x}$Fl for $x=1$ and 2.

The parameters of the model used in the calculation of the reactions ^{208}Pb(^{78}Ge,xn)^{285}Fl are given in Tables 2-4. The values of the parameters are chosen using a similar procedure as before.

The mechanism of compound nucleus formation in this reaction also passes through an intermediate state, see Fig. 2. The inner fission barrier is slightly higher than the outer fission barrier, see Fig. 2. The barrier related to the decay back to the DNS is higher than the inner or outer fission barriers, see Fig. 2 and Tables 3,4. Therefore, the decay of the intermediate state into quasi-fission fragments is more preferential than decays into the compound nucleus or DNS. Due to this we put $P_{is} \approx 0.4$ for a simplification. The decay of the intermediate state into quasi-fission fragments for the reaction ^{208}Pb(^{78}Ge, xn)$^{286-x}$Fl is more probable than for the reaction ^{208}Pb(^{70}Zn,xn)$^{278-x}$Cn.

H. Probability of compound nucleus formation

Let us discuss the mechanisms of compound nucleus formation in our model by comparing the barrier heights of different DNS decay processes. The various barrier heights are given in Tables 1 and 5.

The barrier heights related to the transfer $B^{\rm DNS,tr}_{0,\rm CN}$ and fusion $b^{\rm DNS,f}_{0,\rm CN} = B^{\rm DNS,f}_{0,\rm CN} - Q_{\rm CN}$ paths of the compound nucleus formation obey the inequality $B^{\rm DNS,tr}_{0,\rm CN} > b^{\rm DNS,f}_{0,\rm CN}$. We can conclude from this inequality that $\Gamma^{\rm DNS,tr}_{\rm CN}(E,\ell)=0$ at small collision energies and $\Gamma^{\rm DNS,f}_{\rm CN}(E,\ell) \gg \Gamma^{\rm DNS,tr}_{\rm CN}(E,\ell)$ at high collision energies. Therefore, the transfer mechanism of compound nucleus formation has a small contribution at high collision energies only.

We see in Table 5 that for each reaction the height of the barrier $B^{\rm DNS}_{0,\rm def}$ is the lowest and $B^{\rm DNS,tr}_{0,\rm CN} > b^{\rm DNS,f}_{0,\rm CN}$. Therefore, the values of the widths obey the inequalities $\Gamma^{\rm DNS}_{\rm def}(E,\ell) \gg \Gamma^{\rm DNS,tr}_{\rm CN}(E,\ell)$, $\Gamma^{\rm DNS}_{\rm def}(E,\ell) \gg \Gamma^{\rm DNS}_{\rm DIC}(E,\ell)$, and $\Gamma^{\rm DNS}_{\rm def}(E,\ell) \gg \Gamma^{\rm DNS}_{\rm sph}(E,\ell)$. As a result, $\Gamma^{\rm tot}_{\rm CN}(E,\ell) \approx \Gamma^{\rm DNS}_{\rm def}(E,\ell)$ and the probability of compound nucleus formation may be approximated as

$$P(E,\ell) \approx \frac{\Gamma^{\rm DNS,f}_{\rm CN}(E,\ell)}{\Gamma^{\rm DNS}_{\rm def}(E,\ell)}. \tag{56}$$

At the high excitation energy $E^* = E + Q_{\rm CN}$ of the compound nucleus this expression can be presented in a simple form,

$$\begin{aligned} P(E^*,\ell) &\approx \frac{\Gamma^{\rm DNS,f}_{\rm CN}(E^*,\ell)}{\Gamma^{\rm DNS}_{\rm def}(E^*,\ell)} \\ &\propto \frac{\exp\left\{2\left[a_{\rm dens}\left(E^* - B^{\rm DNS,f}_{0,\rm CN}\right)\right]^{1/2}\right\}}{\exp\left\{2\left[a_{\rm dens}\left(E^* - (B^{\rm DNS}_{0,\rm def} + Q_{\rm CN})\right)\right]^{1/2}\right\}} \\ &\approx \exp\left\{-\left[\frac{a_{\rm dens}}{E^*}\right]^{1/2}\delta_B\right\}, \end{aligned} \tag{57}$$

where $\delta_B = b^{\rm DNS,f}_{0,\rm CN} - B^{\rm DNS}_{0,\rm def}$.

The difference between barriers, δ_B, increases from 6.2 MeV for the reaction ^{50}Ti + ^{208}Pb to 30.4 MeV for the reaction ^{78}Ge + ^{208}Pb, see Table 5. Due to this and Eq. (57), the probability of compound nucleus formation, $P(E^*,\ell)$, strongly decreases with increasing projectile mass, see also Fig. 10. The dependencies of the probabilities of compound nucleus formation $P(E^*,\ell)$ on the excitation energy of the compound nucleus formed in the reactions ^{50}Ti, ^{52,54}Cr, ^{58}Fe, ^{64}Ni, ^{70}Zn, and ^{78}Ge + ^{208}Pb for $\ell=0$ are presented in Fig. 10.

According to the statistical approach, see Eq. (57), the probability of compound nucleus formation increases with rising energy E^*. This rise is very strong at energies near the barrier of compound nucleus formation by fusion. This tendency is clearly seen in Fig. 10. The probability of compound nucleus formation rises more smoothly at higher energies.

Table 5. Barrier height values for the DNS decay branches. $B_0^{\rm fus}$ is the barrier for the DNS decay into the incident channel, $b_{0,\rm CN}^{\rm DNS,f}$ is the barrier for the DNS decay into the compound nucleus by fusion, $B_{0,\rm CN}^{\rm DNS,tr}$ is the barrier for the DNS decay into the compound nucleus by nucleon transfer, $B_{0,\rm DIC}^{\rm DNS}$ is the barrier for the DNS decay into a more symmetric nuclear system than the incident channel, and $B_{0,\rm def}^{\rm DNS}$ is the barrier for DNS decay into the incident deformed nuclei. $\delta_B = b_{0,\rm CN}^{\rm DNS,f} - B_{0,\rm def}^{\rm DNS}$. The barriers are evaluated relative to the nucleus-nucleus interaction energy for an infinite distance between them at $\ell = 0$. All values are given in MeV.

Reactions	$B_0^{\rm fus}$	$b_{0,\rm CN}^{\rm DNS,f}$	$B_{0,\rm CN}^{\rm DNS,tr}$	$B_{0,\rm DIC}^{\rm DNS}$	$B_{0,\rm def}^{\rm DNS}$	δ_B
^{50}Ti + ^{208}Pb	189.8	182.0	198.7	187.1	175.8	6.2
^{52}Cr + ^{208}Pb	207.2	198.4	212.3	199.1	191.3	7.1
^{54}Cr + ^{208}Pb	206.0	198.2	215.7	202.1	189.1	9.1
^{58}Fe + ^{208}Pb	222.0	215.6	232.6	217.5	204.0	11.6
^{64}Ni + ^{208}Pb	236.6	231.1	251.9	233.9	216.2	14.9
^{70}Zn + ^{208}Pb	251.1	246.9	269.3	248.0	228.4	18.5
^{78}Ge + ^{208}Pb	264.4	270.3	289.9	265.4	239.9	30.4

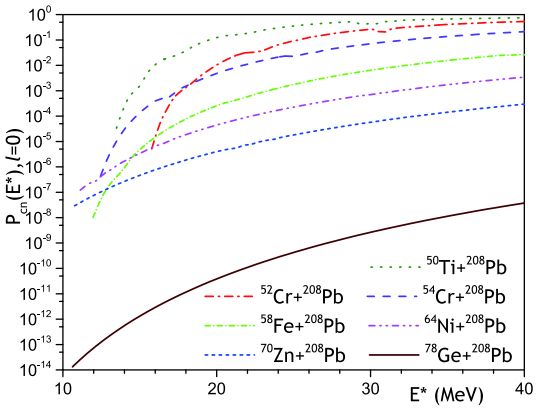

Fig. 10. (color online) Dependencies of the probability of compound nucleus formation on the excitation energy of the compound nucleus formed in reactions ^{50}Ti, ^{52,54}Cr, ^{58}Fe, ^{64}Ni, ^{70}Zn, and ^{78}Ge + ^{208}Pb for $\ell = 0$.

The value of probability $P(E^*,\ell)$ for the reaction ^{78}Ge + ^{208}Pb is much smaller than for the reaction ^{70}Zn + ^{208}Pb, see Fig. 10. This is related to the rise of the difference between barriers δ_B for reactions with ^{78}Ge projectiles, see Table 5. Due to this the cross sections for the reaction ^{78}Ge + ^{208}Pb are much smaller than for the reaction ^{70}Zn + ^{208}Pb; compare the results presented in Figs. 9 and 10.

The values of the barrier height between deformed incident nuclei $B_{0,\rm def}^{\rm DNS,f}$, as well as the width $\Gamma_{\rm def}^{\rm DNS}(E,\ell)$, depend strongly on the surface stiffness coefficient. Therefore, the value of the surface stiffness coefficient strongly affects the probability of compound nucleus formation. Due to this, the choice of incident nuclei is very important for the values of compound nucleus production cross section.

The crucial role of the transfer mechanism of compound nucleus formation in the framework of the DNS model is related to the small height of the barrier $B_{0,\rm CN}^{\rm DNS,tr}$ in this model; see the discussion of this barrier height in Sec. III.F. The DNS path of compound nucleus formation is the main path when $b_{0,\rm CN}^{\rm DNS,f} > B_{0,\rm CN}^{\rm DNS,tr}$. In our model $b_{0,\rm CN}^{\rm DNS,f} < B_{0,\rm CN}^{\rm DNS,tr}$, therefore the fusion path of the compound nucleus production is basic. So, the role of different mechanisms of SHN production depends on the potential landscape, which is defined by the model(s) for the calculation of the potential energy for one- and two-body nuclear shapes.

IV. CONCLUSIONS

We have presented a new model for SHN production in cold-fusion reactions. This model takes into account the competition between the DNS multi-nucleon transfer and fusion trajectories of the compound nucleus formation. The available experimental data are described well by our model.

The compound nucleus is mainly formed by the fusion path, because the barrier related to fusion is lower than the barrier related to multi-nucleon transfer from the light nucleus to the heavy one (the DNS trajectory).

We have shown the correlation between the surface stiffnesses of nuclei involved in SHN production and the reaction cross sections. The use of stiffer nuclei leads to higher cross sections due to reduction of the DNS decay width to deformed nuclei.

The competition between compound nucleus formation and true quasi-fission occurring along the fusion trajectory is taken into account for heavy nucleus-nucleus systems leading to SHN. This competition is related to the existence of an intermediate state and is connected to the landscape of the potential energy surface. The intermediate state is important for reactions with heavy projectiles. The quasi-fission is linked to the decay of the intermediate state into fragments, bypassing the formation of the compound nucleus.

The yields of the various reaction processes in the model depend on the relative values of the corresponding barrier heights. The values of the barrier heights $B_{0,\rm CN}^{\rm DNS,f}$ and $B_{\rm f}$ depend on the choice of the nuclear structure model for calculation of these barriers and the one-body shape parametrization. The uncertainty of the fission barrier height $B_{\rm f}$ obtained in the framework of different models is several MeV, see Table 3. So, we may expect a similar uncertainty for the barrier $B_{0,\rm CN}^{\rm DNS,f}$. The values of the barriers $B_0^{\rm fus}$, $B_{0,\rm CN}^{\rm DNS,tr}$, $B_{0,\rm DIC}^{\rm DNS}$ and $B_{0,\rm def}^{\rm DNS}$ are determined by the choice of the nuclear part of the nucleus-nucleus potential and the stiffness parameter of the nuclei. The

difference between the interaction barrier heights of spherical nuclei leading to SHNs calculated in various approaches to the nuclear interaction part may reach 20 MeV [92]. We emphasize that the barrier values calculated by using the potential (6) agree well with those extracted from quasi-elastic scattering, see Table 1, and with the empirical barriers for light and medium heavy-ion systems [103]. The values of the stiffness parameter are only known for some nuclei. Thus, the obtained results are model-dependent, and the use of more accurate approaches is encouraged in further studies.

ACKNOWLEDGEMENTS

V. Yu. Denisov is grateful to Academician Yu. Ts. Oganessian and Professor S. Hofmann for stimulating discussions. V. Yu. Denisov is grateful to Professor S. Hofmann for a digital form of the experimental data for reactions ^{208}Pb(^{58}Fe, 1*n*)^{265}Hs *and* ^{208}Pb(^{64}Ni, 1*n*)^{271}Ds [12], *which were also presented in Ref.* [41].

References

[1] Yu. Ts. Oganessian, A. Sobiczewski, and G. M. Ter-Akopian, Phys. Scr. **92**, 023003 (2017)
[2] S. Hofmann and G. Munzenberg, Rev. Mod. Phys. **72**, 733 (2000)
[3] S. Hofmann, Russian Chemical Reviews **78**, 1123 (2009)
[4] S. Hofmann, J. Phys. G **42**, 114001 (2015)
[5] Yu. Ts. Oganessian *et al*., Phys. Rev. C **64**, 054606 (2001)
[6] A. V. Belozerov *et al*., Eur. Phys. J. A **16**, 447 (2003)
[7] F. P. Hessberger *et al*., Z. Phys. A **359**, 415 (1997)
[8] J. Khuyagbaatar *et al*., Nucl. Phys. A **994**, 121662 (2020)
[9] I. Dragojevic *et al*., Phys. Rev. C **78**, 024605 (2008)
[10] B. Streicher *et al*., Eur. Phys. J. A **45**, 275 (2010)
[11] C. M. Folden *et al*., Phys. Rev. C **79**, 027602 (2009)
[12] S. Hofmann, privite communications
[13] N. Sato *et al*., J. Phys. Soc. Japan **80**, 094201 (2011)
[14] K. Morita *et al*., Eur. Phys. J. A **21**, 257 (2004)
[15] T. N. Ginter *et al*., Phys. Rev. C **67**, 064609 (2003)
[16] S. Hofmann *et al*., Eur. Phys. J. A **14**, 147 (2002)
[17] K. Morita *et al*., J. Phys. Soc. Jpn. **76**, 043201 (2007)
[18] T. Sumita *et al*., J. Phys. Soc. Jpn. **82**, 024202 (2013)
[19] C. M. Folden, *Development of Odd-Z-Projectile Reactions for Transactinide Element Synthesis*, PhD-Thesis, (Berkeley: Univeristy of California, USA 2004) DOI: 10.2172/843003
[20] K. Morita *et al*., J. Phys. Soc. Jpn. **73**, 1738 (2004)
[21] K. Morita *et al*., J. Phys. Soc. Jpn. **73**, 2593 (2004)
[22] K. Morita, Nucl. Phys. A **944**, 30 (2015)
[23] V. K. Utyonkov *et al*., Phys. Rev. C **97**, 014320 (2018)
[24] Yu. Ts. Oganessian *et al*., Phys. Rev. C **74**, 044602 (2006)
[25] N. T. Brewer *et al*., Phys. Rev. C **98**, 024317 (2018)
[26] M. Schadel, *The chemistry of super-heavy elements*, (Kluwer Academic Publishers, Dordrecht, 2003)
[27] V. Yu. Denisov and V. A. Plujko, *Problems of physics of atomic nucleus and nuclear reactions,* (Publishing and Polygraphic Centre "The University of Kiev", Kiev, 2013) (in Russian)
[28] R. W. Lougheed *et al*., Phys. Rev. C **32**, 1760 (1985)
[29] Yu. Ts. Oganessian *et al*., Phys. Rev. C **79**, 024603 (2009)
[30] E. M. Kozulin *et al*., Phys. Lett. B **686**, 227 (2010)
[31] S. Hofmann *et al*., Eur. Phys. J. A **52**, 180 (2016)
[32] F. P. Hessberger and D. Ackermann, Eur. Phys. J. A **53**, 123 (2017)
[33] A. Di Nitto *et al*., Phys. Lett. B **784**, 199 (2018)
[34] K. V. Novikov *et al*., Bull. Russ. Acad. Sci. Physics **84**, 495 (2020)
[35] Yu. Ts. Oganessian *et al*., Nucl. Phys. A **239**, 353 (1975)
[36] W. J. Swiatecki, Phys. Ser. **24**, 113 (1981)
[37] W. J. Swiatecki, Nucl. Phys. A **376**, 275 (1982)
[38] S. Bjornholm and W. J. Swiatecki, Nucl. Phys. A **391**, 471 (1982)
[39] J. P. Blocki, H. Feldmeier, and W. Swiatecki, Nucl. Phys. A **459**, 145 (1986)
[40] Y. Aritomo *et al*., Phys. Rev. C **59**, 796 (1999)
[41] V. Yu. Denisov and S. Hofmann, Phys. Rev. C **61**, 034606 (2000)
[42] V. Yu. Denisov, Prog. Part. Nucl. Phys. **46**, 303 (2001)
[43] C. Shen, G. Kosenko, and Y. Abe, Phys. Rev. C **66**, 061602 (2002)
[44] W. J. Swiatecki, K. Siwek-Wilczynska, and J. Wilczynski, Phys. Rev. C **71**, 014602 (2005)
[45] G. I. Kosenko *et al*., Phys. At. Nucl. **71**, 2052 (2008)
[46] T. Cap, K. Siwek-Wilczynska, and J. Wilczynski, Phys. Rev. C **83**, 054602 (2011)
[47] D. Boilley *et al*., Phys. Rev. C **84**, 054608 (2011)
[48] Y. Aritomo *et al*., Phys. Rev. C **85**, 044614 (2012)
[49] Yu-Jie Min Zhu, Zu-Hua Liu, and Wen-Zhong Wang, Phys. Rev. C **86**, 037602 (2012)
[50] K. Siwek-Wilczynska *et al*., Phys. Scr. T **154**, 014005 (2013)
[51] V. I. Zagrebaev and W. Greiner, Nucl. Phys A **944**, 257 (2015)
[52] A. S. Umar and V. E. Oberacker, Nucl. Phys. A **944**, 238 (2015)
[53] A. S. Umar, V. E. Oberacker, and C. Simenel, Phys. Rev. C **94**, 024605 (2016)
[54] M. Tohyama and A. S. Umar, Phys. Rev. C **93**, 034607 (2016)
[55] H. Lu *et al*., Phys. Rev. C **94**, 034616 (2016)
[56] V. L. Litnevsky *et al*., Phys. Rev. C **101**, 064616 (2020)
[57] A. Diaz-Torres, Phys. Rev. C **69**, 021603 (2004)
[58] A. Diaz-Torres, Phys. Rev. C **74**, 064601 (2006)
[59] V. V. Volkov, Izv. Akad. Nauk SSSR, Ser. Fiz. **50**, 1879 (1986)
[60] N. V. Antonenko *et al*., Phys. Lett. B **319**, 425 (1993)
[61] N. V. Antonenko *et al*., Phys. Rev. C **51**, 2635 (1995)
[62] G. G. Adamian *et al*., Nucl. Phys. A **633**, 409 (1998)
[63] G. G. Adamian, N. V. Antonenko, and W. Scheid, Nucl. Phys. A **678**, 24 (2000)
[64] V. V. Volkov, Physics of Part. and Nuclei **35**, 425 (2004)
[65] Z. H. Liu and J. D. Bao, Phys. Rev. C **74**, 057602 (2006)
[66] Z. Q. Feng *et al*., Nucl. Phys A **771**, 50 (2006)
[67] Z. Q. Feng *et al*., Phys. Rev. C **76**, 044606 (2007)
[68] N. Wang, E. G. Zhao, and W. Scheid, Phys. Rev. C **89**, 037601 (2014)
[69] L. Zhu *et al*., Phys. Rev. C **90**, 014612 (2014)

[70] X. J. Bao *et al*., Phys. Rev. C **93**, 044615 (2016)
[71] G. G. Adamian *et al*., Phys. Rev. C **96**, 044310 (2017)
[72] Zhi-Han Wu and Long Zhu, Phys. Rev. C **97**, 064609 (2018)
[73] Fan Li *et al*., Phys. Rev. C **98**, 014618 (2018)
[74] Jingjing Li *et al*., Phys. Rev. C **98**, 014626 (2018)
[75] G. Giardina *et al*., Nucl. Phys. A **970**, 169 (2018)
[76] X. J. Bao, Chinese Phys. C **43**, 054105 (2019)
[77] L. Zhu, Chinese Phys. C **43**, 124103 (2019)
[78] G. G. Adamian *et al*., Eur. Phys. J. A **56**, 47 (2020)
[79] W. Loveland, Phys. Rev. C **76**, 014612 (2007)
[80] W. Loveland, Eur. Phys. J. A **51**, 120 (2015)
[81] V. Zagrebaev and W. Greiner, Phys. Rev. C **78**, 034610 (2008)
[82] R. Smolanczuk, Phys. Rev. C **81**, 067602 (2010)
[83] R. K. Choudhury and Y. K. Gupta, Phys. Lett. B **731**, 168 (2014)
[84] K. N. Sridhar, H. C. Manjunatha, and H. B. Ramalingam, Nucl. Phys. A **983**, 195 (2019)
[85] H. C. Manjunatha, K. N. Sridhar, and N. Sowmya, Nucl. Phys. A **987**, 382 (2019)
[86] K. P. Santhosh and V. Safoora, J. Phys. G **44**, 125105 (2017)
[87] K. Hagino, Phys. Rev. C **98**, 014607 (2018)
[88] T. V. Nhan Hao *et al*., Int. J. Mod. Phys. E **28**, 1950056 (2019)
[89] A. Diaz-Torres *et al*., Phys. Lett. B **481**, 228 (2020)
[90] V. V. Volkov, Phys. Rep. **44**, 93 (1978)
[91] V. Yu. Denisov and W. Norenberg, Eur. Phys. J. A **15**, 375 (2002)
[92] V. Yu. Denisov and V. A. Nesterov, Phys. At. Nucl. **69**, 1472 (2006)
[93] D. Berdichevsky, A. Lukasiak, W. Norenberg *et al*., Nucl. Phys. A **499**, 609 (1989)
[94] P. Moller *et al*., At. Data Nucl. Data Tabl. **109-110**, 1 (2016)
[95] V. Yu. Denisov and N. A. Pilipenko, Phys. Rev. C **76**, 014602 (2007)
[96] V. Yu. Denisov and N. A. Pilipenko, Phys. Rev. C **81**, 025805 (2010)
[97] V. Yu. Denisov, T. O. Margitych, and I. Yu. Sedykh, Nucl. Phys. A **958**, 101 (2017)
[98] V. Yu. Denisov and I. Yu. Sedykh, Nucl. Phys. A **963**, 15 (2017)
[99] V. Yu. Denisov, N. A. Pilipenko, and I. Yu. Sedykh, Phys. Rev. C **95**, 014605 (2017)
[100] D. L. Hill and J. A. Wheeler, Phys. Rev. **89**, 1102 (1953)
[101] M. Dasgupta *et al*., Annu. Rev. Nucl. Part. Sci. **48**, 401 (1998)
[102] G. Montagnoli and A. M. Stefanini, Eur. Phys. J. A **53**, 169 (2017)
[103] V. Yu. Denisov, Phys. Rev. C **91**, 024603 (2015)
[104] V. M. Strutinsky, Sov. J. Nucl. Phys. **3**, 449 (1966)
[105] V. M. Strutinsky, Nucl. Phys. A **95**, 420 (1967)
[106] V. M. Strutinsky, Nucl. Phys. A **122**, 1 (1968)
[107] M. Brack *et al*., Rev. Mod. Phys. **44**, 320 (1972)
[108] G. Audi *et al*., Chinese Physics C **41**, 030001 (2017)
[109] R. Bass, Lecture Notes in Physics **117**, 281 (1980)
[110] J. O. Newton *et al*., Phys. Rev. C **70**, 024605 (2004)
[111] I. Dutt and R. K. Puri, Phys. Rev. C **81**, 064608 (2010)
[112] S. Mitsuoka *et al*., Phys. Rev. Lett **99**, 182701 (2007)
[113] V. Yu. Denisov, Eur. Phys. J. A **7**, 87 (2000)
[114] V. Yu. Denisov and I. Yu. Sedykh, Eur. Phys. J. A **55**, 153 (2019)
[115] P. Frobrich and R. Lipperheide, *Theory of Nuclear Reactions,* (Clarendon Press, Oxford, 1996)
[116] N. Bohr and J. A. Wheeler, Phys. Rev. **56**, 426 (1939)
[117] D. A. Varshalovich, A. N. Moskalev, and V. K. Khersonsky, *Quantum Theory of Angular Momentum: Irreducible Tensors*, Spherical Harmonics, Vector Coupling Coefficients, 3nj Symbols (World scientific, Singapore, 1988)
[118] R. W. Hasse and W. D. Myers, *Geometrical relationships of macroscopic nuclear physics* (Springer-Verlag, Berlin, 1988)
[119] S. Cwiok *et al*., Comput. Phys. Commun. **46**, 379 (1987)
[120] H. J. Lipkin, Ann. Phys. N. Y. **9**, 272 (1960)
[121] P. Möller and J. R. Nix, Nucl. Phys. A **361**, 117 (1981)
[122] R. Smolanczuk, J. Skalski, and A. Sobiczewski, Phys. Rev. C **52**, 1871 (1995)
[123] R. Smolanczuk, Phys. Rev. **56**, 812 (1997)
[124] M. Kowal, P. Jachimowicz, and J. Skalski, arXiv: 1203.5013v1 [nucl-th] 22 Mar 2012
[125] S. Bjornholm and V. M. Strutinsky, Nucl. Phys. A **136**, 1 (1969)
[126] S. Bjornholm and J. E. Lynn, Rev. Mod. Phys. **52**, 725 (1980)
[127] A. Mamdouh *et al*., Nucl. Phys. A **679**, 337 (2001)
[128] V. Yu. Denisov, Phys. At. Nucl. **68**, 1133 (2005)
[129] J. A. Sheikh, W. Nazarewicz, and J. C. Pei, Phys. Rev. C **80**, 011302 (2009)
[130] J. C. Pei *et al*., Phys. Rev. Lett. **102**, 192501 (2009)
[131] J. C. Pei *et al*., Nucl. Phys. A **834**, 381c (2010)
[132] M. Kowal, P. Jachimowicz, and A. Sobiczewski, Phys. Rev. C **82**, 014303 (2010)
[133] H. Abusara, A. V. Afanasjev, and P. Ring, Phys. Rev. C **85**, 024314 (2012)
[134] M. Warda and J. L. Egido, Phys. Rev. C **86**, 014322 (2012)
[135] P. Moller *et al*., Phys. Rev. C **91**, 024310 (2015)
[136] P. Jachimowicz, M. Kowal, and J. Skalski, Phys. Rev. C **95**, 014303 (2017)
[137] S. E. Agbemava *et al*., Phys. Rev. **92**, 054310 (2015)
[138] S. E. Agbemava *et al*., Phys. Rev. C **95**, 054324 (2017)
[139] M. Warda, A. Zdeb, and L. M. Robledo, Phys. Rev. C **98**, 041602(R) (2018)
[140] P. Moller *et al*., Z. Phys. A **359**, 251 (1997)
[141] P. Moller *et al*., J. Nucl. Sci. Tech. **39**(supl. 2), 703 (2002)
[142] I. M. Itkis *et al*., Nucl. Phys. A **734**, E29 (2004)
[143] I. M. Itkis *et al*., Nucl. Phys. A **787**, 150c (2007)
[144] I. M. Itkis *et al*., Phys. Rev. C **83**, 064613 (2011)
[145] R. Capote *et al*., Nuclear Data Sheets, **110**: 3107 (2009); http://www-nds.iaea.org/RIPL-3/
[146] A. V. Ignatyuk, G. N. Smirenkin, and A. S. Tishin, Sov. J. Nucl. Phys. **21**, 255 (1975)
[147] W. D. Myers and W. J. Swiatecki, Nucl. Phys. **81**, 1 (1966)
[148] V. Yu. Denisov, Phys. At. Nucl. **70**, 244 (2007)
[149] V. Yu. Denisov and N. A. Pilipenko, Phys. At. Nucl. **73**, 1152 (2010)
[150] V. Yu. Denisov and T. O. Margitych, J. Nucl. Phys. At. Energy **15**, 119 (2014)
[151] V. Yu. Denisov and T. O. Margitych, Ukr. J. Phys. **60**, 585 (2015)
[152] V. Yu. Denisov and T. O. Margitych, Reports Nat. Acad. Sci. Ukraine **4**, 57 (2015)

[153] B. V. Derjaguin, Kolloid-Zeitschrift **69**, 155 (1934)
[154] J. Blocki *et al*., Ann. Phys. **105**, 427 (1977)
[155] M. Ismail and I. A. M. Abdul-Magead, Nucl. Phys. A **922**, 168 (2012)
[156] A. Bohr and B. Mottelson, Nuclear structure, Vol. 2 (W. A. Benjamin Inc. : New York, Amsterdam, 1974)
[157] C. Y. Wong, Nucl. Data A **4**, 271 (1968)
[158] B. Pritychenko *et al*., At. Data Nucl. Data Tabl. **107**, 1 (2016)
[159] T. Kibedi and R. H. Spear, At. Data Nucl. Data Tabl. **80**, 35 (2002)
[160] V. Yu. Denisov and I. Yu. Sedykh, Phys. Rev. C **98**, 024601 (2018)
[161] G. D. Adeev and P. A. Cherdantsev, Phys. Lett. B **39**, 485 (1972)
[162] G. D. Adeev and P. A. Cherdantsev, Sov. J. Nucl. Phys. **18**, 381 (1974)
[163] M. Brack, Ph. Quentin, Phys. Scripta A **10**, 163 (1974)
[164] M. Diebel, K. Albrecht, and R. W. Hasse, Nucl. Phys. A **55**, 66 (1981)
[165] Z. Lojewski, V. V. Pashkevich, and S. Cwiok, Nucl. Phys. A **436**, 499 (1985)
[166] Yi Zhu and J. C. Pei, Phys. Rev. C **94**, 024329 (2016)
[167] J. D. Jackson, Can. J. Phys. **34**, 767 (1956)
[168] R. Vandenbosch and J. R. Huizenga, Nuclear Fission (New York, Academic Press, 1973)
[169] M. Pi, X. Vinnas, and M. Barranco, Phys. Rev. C **26**, 733 (1982)
[170] M. Brack, C. Guet, and H.-B. Hakannson, Phys. Rep. **123**, 275 (1985)
[171] C. Guet, E. Strumberger, and M. Brack, Phys. Lett. B **205**, 427 (1988)
[172] W. J. Swiatecki, K. Siwek-Wilczynska, and J. Wilczynski, Phys. Rev. C **78**, 054604 (2008)
[173] W. J. Swiatecki, K. Siwek-Wilczynska, and J. Wilczynski, Phys. Rev. C **81**, 019804 (2010)